

Accepted Manuscript

Synthesis and Evaluation of Novel Potent TSPO PET Ligands with 2-Phenylpyrazolo[1,5-*a*]pyrimidin-3-yl Acetamide

Van Hieu Tran, Hyunjun Park, Jaekyung Park, Young-Do Kwon, Shinwoo Kang, Jae Ho Jung, Keun-A Chang, Byung Chul Lee, Sang-Yoon Lee, Soosung Kang, Hee-Kwon Kim

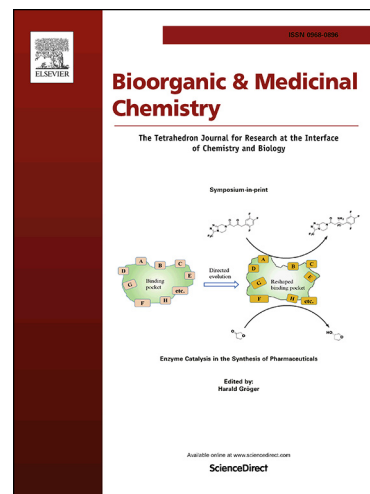
PII: S0968-0896(19)30637-6
DOI: <https://doi.org/10.1016/j.bmc.2019.07.036>
Reference: BMC 15020

To appear in: *Bioorganic & Medicinal Chemistry*

Received Date: 24 April 2019
Revised Date: 9 July 2019
Accepted Date: 19 July 2019

Please cite this article as: Hieu Tran, V., Park, H., Park, J., Kwon, Y-D., Kang, S., Ho Jung, J., Chang, K-A., Chul Lee, B., Lee, S-Y., Kang, S., Kim, H-K., Synthesis and Evaluation of Novel Potent TSPO PET Ligands with 2-Phenylpyrazolo[1,5-*a*]pyrimidin-3-yl Acetamide, *Bioorganic & Medicinal Chemistry* (2019), doi: <https://doi.org/10.1016/j.bmc.2019.07.036>

This is a PDF file of an unedited manuscript that has been accepted for publication. As a service to our customers we are providing this early version of the manuscript. The manuscript will undergo copyediting, typesetting, and review of the resulting proof before it is published in its final form. Please note that during the production process errors may be discovered which could affect the content, and all legal disclaimers that apply to the journal pertain.



Synthesis and Evaluation of Novel Potent TSPO PET Ligands with 2-Phenylpyrazolo[1,5-*a*]pyrimidin-3-yl Acetamide

Van Hieu Tran ^{a,‡}, Hyunjun Park ^{b,c,d,‡}, Jaekyung Park ^e, Young-Do Kwon ^f, Shinwoo Kang ^{b,c}, Jae Ho Jung ^{g,h},
Keun-A Chang ^{b,c,d}, Byung Chul Lee ^{g,h}, Sang-Yoon Lee ^{c,e,i}, Soosung Kang^j, Hee-Kwon Kim ^{a,k *}

^[a] Department of Nuclear Medicine, Molecular Imaging & Therapeutic Medicine Research Center, Chonbuk National University Medical School and Hospital, Jeonju 54907, Republic of Korea

^[b] Department of Pharmacology, College of Medicine, Gachon University, Incheon 21936, Republic of Korea

^[c] Neuroscience Research Institute, Gachon University, Incheon 21565, Republic of Korea

^[d] Department of Health Sciences and Technology, Gachon Advanced Institute for Health Sciences and Technology (GAIHST), Gachon University, Incheon 21999, Republic of Korea

^[e] Gachon Advanced Institute for Health Sciences and Technology, Graduate School, Gachon University, Incheon 21936, Republic of Korea

^[f] Department of Nuclear Medicine, Yonsei University College of Medicine, Seoul 03722, Republic of Korea

^[g] Department of Nuclear Medicine, Seoul National University College of Medicine, Seoul National University Bundang Hospital, Seongnam 13620, Republic of Korea

^[h] Center for Nanomolecular Imaging and Innovative Drug Development, Advanced Institutes of Convergence Technology, Suwon 16229, Republic of Korea

^[i] Department of Neuroscience, College of Medicine, Gachon University, Incheon 21936, Republic of Korea

^[j] College of Pharmacy and Graduate School of Pharmaceutical Sciences, Ewha Womans University, Seoul 03760, Republic of Korea

^[k] Research Institute of Clinical Medicine of Chonbuk National University-Biomedical Research Institute of Chonbuk National University Hospital, Jeonju 54907, Republic of Korea

[‡] These authors contributed equally.

* Corresponding author.

Tel: +82 63 250 2768; Fax: +82 63 255 1172.

E-mail address: hkkim717@jbnu.ac.kr (H-K Kim).

Postal address: Department of Nuclear Medicine, Chonbuk National University Medical School, Geonji-ro 20, Deokjin-gu, Jeonju, Jeonbuk 54907, Republic of Korea

ABSTRACT

Translocator protein (TSPO) expression is closely related with neuroinflammation and neuronal damage which might cause several central nervous system diseases. Herein, a series of TSPO ligands (**11a–c** and **13a–d**) with a 2-phenylpyrazolo[1,5-*a*]pyrimidin-3-yl acetamide structure were prepared and evaluated via an *in vitro* binding assay. Most of the novel ligands exhibited a nano-molar affinity for TSPO, which was better than that of DPA-714. Particularly, **11a** exhibited a subnano-molar TSPO binding affinity with suitable lipophilicity for *in vivo* brain studies. After radiolabeling with fluorine-18, [¹⁸F]**11a** was used for a dynamic positron emission tomography (PET) study in a rat LPS-induced neuroinflammation model; the inflammatory lesion was clearly visualized with a superior target-to-background ratio compared to [¹⁸F]DPA-714. An immunohistochemical examination of the dissected brains confirmed that the uptake location of [¹⁸F]**11a** in the PET study was consistent with a positively activated microglia region. This study proved that [¹⁸F]**11a** could be employed as a potential PET tracer for detecting neuroinflammation and could give possibility for diagnosis of other diseases, such as cancers related with TSPO expression.

Keywords: Translocator protein; Positron emission tomography probe; Structure activity relationships; Neuroinflammation.

1. Introduction

Positron emission tomography (PET) is a noninvasive molecular imaging technique that can provide crucial information including disease progress and biochemical events. In a PET image study, radiopharmaceuticals containing a positron emitter were employed.¹⁻⁴ Widely used positron-emitting radionuclides for PET include ^{11}C ($t_{1/2} = 20.4$ min), ^{13}N ($t_{1/2} = 9.97$ min), ^{15}O ($t_{1/2} = 2.04$ min), and ^{18}F ($t_{1/2} = 110$ min), which are produced from cyclotrons. Specially, fluorine-18 offers several advantages such as a long half-life and low-energy positron (0.635 MeV) compared to the other cyclotron-produced radionuclides; fluorine-18 is adequate to high resolution PET imaging, multistep synthesis, and transportation to research centers and hospitals. In this sense, various ^{18}F -labeled radiotracers have been developed to study biologically important targets of interest using PET modality.^{4,5}

One biological target in medical studies is the 18-kDa translocator protein (TSPO), which was previously named as a peripheral type benzodiazepine receptor.⁶ Although TSPO is highly expressed in many cell types related to steroidogenesis, it has been reported that TSPO expression in the brain is restricted to microglia and astrocytes.^{7,8} Microglial cells are resident macrophages in the central nervous system (CNS); their activation resulting from endogenous or exogenous signals such as bacterial lipopolysaccharide (LPS) is involved in CNS inflammation.^{8,9} Additionally, there are several reports that astrocytes are activated and related to neuroinflammation.⁸⁻¹⁰ Because TSPO overexpression in the CNS is caused by microglial activation, TSPO has been considered as an important biomarker for CNS diseases such as Parkinson's disease and Alzheimer's disease.⁸⁻¹¹

Since [^{11}C]PK11195 was first reported to detect diseases associated with TSPO expression,^{12,13} it has been widely studied and used as a TSPO PET ligand; however, several studies have demonstrated critical limitations, such as a low signal to noise ratio and poor brain uptake.¹⁴⁻¹⁶ Moreover, [^{11}C]PK11195 used carbon-11 which possesses a short half-life

for PET imaging studies. Such hindrances and the advantages of fluorine-18 have led research groups to develop new ^{18}F -labeled TSPO PET imaging agents such as ^{18}F]FEDAA1106,¹⁷ ^{18}F]DPA-714,¹⁸ ^{18}F]AB5186,¹⁹ ^{18}F]GE-180,²⁰ and ^{18}F]FEPPA.²¹ Among them, ^{18}F]DPA-714 is a promising TSPO PET ligand with a high binding affinity and has also been most extensively investigated and employed in preclinical to clinical studies.^{22–25} Various derivatives from structure activity relationship (SAR) studies with 2-phenylpyrazolo[1,5-*a*]pyrimidin-3-yl acetamide scaffold, the core chemical structure of DPA-714, have been reported to establish improved radiotracers for TSPO.^{26–31} However, very few 2-phenylpyrazolo[1,5-*a*]pyrimidin-3-yl acetamide based ligands have exhibited both high TSPO binding affinity and proper lipophilicity for brain studies. Recently, we also reported several TSPO PET probes with the scaffold; one of our previously reported ligands exhibited comparable TSPO binding affinity and an improved relative uptake of ipsilateral areas administrated with LPS compared to the contralateral areas than those of ^{18}F]DPA-714.³² However, it also possesses a high lipophilicity even though PET images in animal brains were successfully obtained using a micro PET study.

To overcome this limitation, we tried to design novel ligands with a much higher TSPO binding affinity and more suitable lipophilicity for brain PET studies through the modification of substituents of the 2-phenylpyrazolo[1,5-*a*]pyrimidin-3-yl acetamide scaffold. Here, new TSPO ligands bearing branched aliphatic groups and cyclic groups based on 2-phenylpyrazolo[1,5-*a*]pyrimidin-3-yl acetamide were prepared, and *in vitro* experiments were performed to measure their binding affinity with TSPO. Newly synthesized ligands exhibiting a higher *in vitro* binding affinity to TSPO and suitable lipophilicity from the SAR study were employed to perform *in vivo* animal PET studies. Through *in vivo* brain studies, the novel ligand was proven to be a promising PET imaging probe for TSPO.

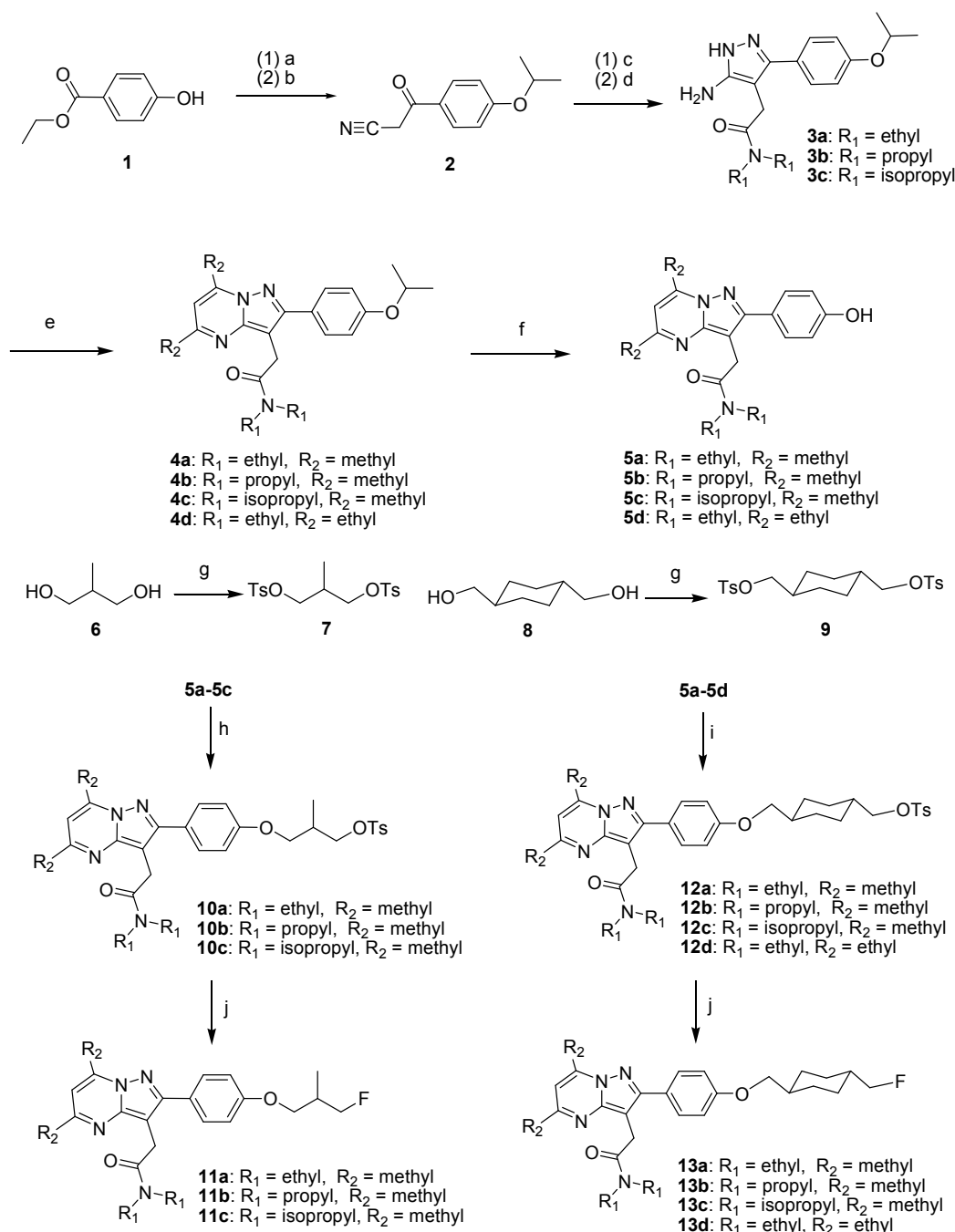
2. Results and discussion

2.1. Chemistry

As shown in Scheme 1, 2-(5,7-dialkyl-2-(4-hydroxyphenyl)pyrazolo[1,5-*a*]pyrimidin-3-yl)-*N,N*-dialkylacetamides (**5a–d**) were prepared via modifications in our previously reported method.³²

A starting material, commercially obtained ethyl 4-hydroxybenzoate **1** was protected with an isopropyl ether and treated with acetonitrile in the presence of potassium *tert*-butoxide to yield a beta-ketonitrile derivative (**2**). Alpha carbon deprotonation of the ketone of **2** to the enolate followed by treatment with hydrazine monohydrate afforded aminopyrazoles (**3a–c**). Condensation of **3a–c** with acetylacetone or 3,5-heptanedione yielded the pyrazolopyrimidine motif (**4a–d**); subsequent removal of the isopropyl of **4a–d** in the presence of aluminum chloride generated **5a–d**. After dialcohols (**6** and **8**) were treated with *p*-toluenesulfonyl chloride to yield the corresponding ditosylates (**7** and **9**), each ditosylate (**7** or **9**) was reacted with the phenol group of **5a–d** in the presence of potassium carbonate to yield precursors (**10a–c** and **12a–d**) with a 64–80% yield. The reaction of **10a–c** or **12a–d** with tetrabutylammonium fluoride hydrate yielded the corresponding new fluoro based TSPO ligand compounds (**11a–c** and **13a–d**) with an 81–96% yield.

Scheme 1. Synthetic route toward novel TSPO ligands.



Reagents and conditions. a) 2-Bromopropane, potassium carbonate, acetone, reflux, 3 days. b) Acetonitrile, potassium *tert*-butoxide, tetrahydrofuran, rt, 2 h. c) Sodium hydride, 2-bromo-*N,N*-diethylacetamide or 2-bromo-*N,N*-dipropylacetamide or 2-bromo-*N,N*-diisopropylacetamide, tetrahydrofuran, rt, 21–22 h. d) Hydrazine monohydrate, acetic acid, ethanol, reflux, 13–14 h. e) 2,4-Pentanedione or 3,5-heptanedione, ethanol, reflux, 14–16 h. f) Aluminum chloride, dichloromethane, rt, 14–16 h. g) *p*-Toluenesulfonyl chloride, triethylamine, dichloromethane, rt, 15–18 h. h) Compound **7**, potassium carbonate, acetonitrile, 60 °C, 19–23 h. i) Compound **9**, potassium carbonate, acetonitrile, 60 °C, 12–14 h. j) Tetrabutylammonium fluoride hydrate, 2-methyl-2-butanol, 80 °C, 12–15 h.

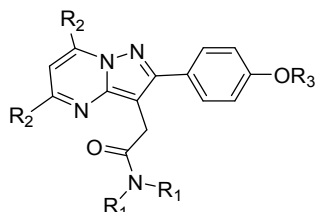
2.2 *In vitro* binding assay and lipophilicity

Newly prepared ligands (**11a–c** and **13a–d**) were used to evaluate the *in vitro* TSPO binding affinities (K_i) via a competition study with [^3H]PK11195. All new ligands exhibited a better binding affinity to TSPO compared with DPA-714 (Table 1). TSPO ligands **11a** with a branched aliphatic structure and **13a** with a cyclic hexyl group at R_3 position, each bearing an ethyl group at R_1 , yielded 3.5- and 2.4- fold higher affinity to TSPO compared with DPA-714, respectively: The K_i values of **11a** and **13a** were 0.94 nM and 1.32 nM, respectively. These results indicated that a branched aliphatic structure at the R_3 position provided a more positive binding affinity to TSPO compared with a cyclic structure at the R_3 position. In addition, affinities were found to increase as smaller moieties were introduced at the R_1 position: ethyl- (**11a** and **13a**) > propyl- (**11b** and **13b**) > isopropyl- (**11c** and **13c**). This result indicated that the binding affinity to TSPO was also influenced by a substituent at the R_1 position. It was noted that, when an isopropyl group (branched) was introduced to the R_1 position, the binding affinity to TSPO was improved compared with an *n*-propyl group (linear) at the R_1 position.

The lipophilicity ($\log P_{7.5}$) of compounds is an important factor in brain studies because it can indicate penetration of the brain-blood barrier in the brain and thus can be used as an indirect indicator. The $\log P_{7.5}$ of the newly prepared ligands (**11a–c** and **13a–d**) was examined using a previously reported method.³² As shown in Table 1, $\log P_{7.5}$ values were affected by ligand substituents and ranged between 2.44 and 3.92. It was found that a (4-(fluoromethyl)cyclohexyl)methoxy group at the R_3 position yielded a higher lipophilicity than a 3-fluoro-2-methylpropoxy group at the R_3 position; propyl and isopropyl groups at the R_1 position yielded higher lipophilicity values than ethyl groups at the R_1 position. Improved lipophilicity results were observed for ethyl groups at the R_2 position compared with methyl groups at the R_2 position. Among the new ligands, **11a** and **11c** exhibited lower lipophilicity

(log $P_{7.5}$ for **11a** = 2.44, and log $P_{7.5}$ for **11c** = 2.93) compared with the other new ligands, suggesting that **11a** and **11c** possessed more suitable log $P_{7.5}$ values for *in vivo* brain studies.

Table 1. Chemical characteristic and binding affinity values of the new TSPO ligands and reference compound



Compound	R ₁	R ₂	R ₃	K _i (nM ± SD) ^a	LogP _{7.5}
DPA-714	-Et	-Me	-CH ₂ CH ₂ F	3.26 ± 0.390	1.99
11a	-Et	-Me	-CH ₂ CH(CH ₃)CH ₂ F	0.94 ± 0.045	2.44
11b	-Pr	-Me	-CH ₂ CH(CH ₃)CH ₂ F	1.11 ± 0.074	3.17
11c	-iPr	-Me	-CH ₂ CH(CH ₃)CH ₂ F	1.04 ± 0.065	2.93
11d^b	-Et	-Et	-CH ₂ CH(CH ₃)CH ₂ F	3.12 ± 0.065	3.21
13a	-Et	-Me	-CH ₂ C ₆ H ₁₀ CH ₂ F	1.32 ± 0.067	3.34
13b	-Pr	-Me	-CH ₂ C ₆ H ₁₀ CH ₂ F	1.88 ± 0.072	3.92
13c	-iPr	-Me	-CH ₂ C ₆ H ₁₀ CH ₂ F	1.59 ± 0.093	3.73
13d	-Et	-Et	-CH ₂ C ₆ H ₁₀ CH ₂ F	2.39 ± 0.054	3.91

^a The mean ± SD of three experiments.

^b See reference 32.

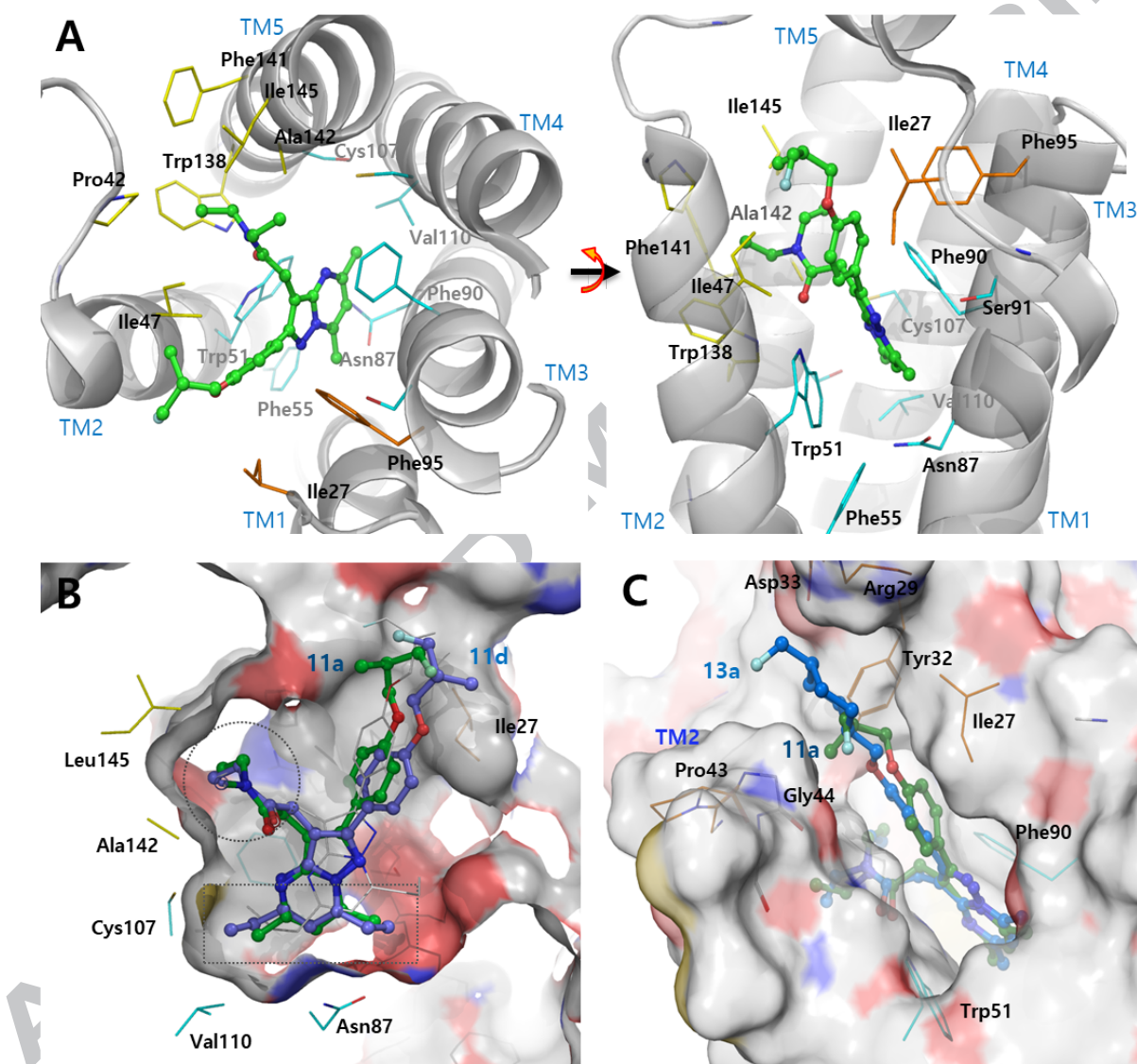
2.3. Modeling docking study

Molecular docking is a study used to predict the mode of action of novel compounds when binding with target proteins. TSPO is comprised of five transmembrane helices (TM1–5) with a short extra-membranous helix ($\alpha_{1,2}$) between TM1 and TM2. The 3D

structures of the TSPO-PK11195 complex (PDB: 4RYI, 2MGY) showed the drug binding site is in the upper cytosolic part of the five transmembrane helical bundles.³³⁻³⁴ Newly prepared compounds were docked into the PK11195 binding site (PDB: 4RYI) using the Glide module of the Schrödinger software with the Maestro interface. As shown in Fig. 1a-b, the pyrazolopyrimidine of **11a** and **11d** was located in a PK11195 binding pocket formed by Trp51, Phe55, Asn87, Phe90, Ser91, Cys107 and Val110. Interestingly, the aromatic residues of Trp51 and Phe90 in the pocket were involved in π - π stacking interaction with the pyrazolopyrimidine of the inhibitors. This pocket appears to only fit with methyl- or ethyl-substituted pyrazolopyrimidines, docking analysis with a propyl-substituted dummy derivative (white molecule in Fig. 1b) showed altered positioning at the binding pocket with worse docking score. The *N,N*-dialkyl amide chain of the synthesized molecules contacts Pro42, Ile47, Phe90, Trp138, Phe 141, Ala142, Leu145, and Ser146. Apparently, steric repulsion between *N*-alkyl group of the amide and hydrophobic residues on the binding site can destabilize the binding. Docking simulations with the newly prepared compounds as well as with more bulky dummy amides indicated that the particular *N*-diethyl or *N*-diisopropyl substitution on the amide is subjected to minimal repulsive interactions in the TSPO amide binding site. The repulsive interaction between bulky amides and TSPO slightly altered the position of the pyrazolopyrimidine and middle aromatic ring to limit retention of the fluoroalkyl ether group to the originally occupied binding site. This negative modulation was more severe when a bulky fluoroalkyl group was utilized as an ether moiety (**13a-d**). In additions, the 4-(fluoromethyl)cyclohexyl group on 13a-d was partially outside the drug binding site, and probably should pay solvation penalty during exposure to a biological solvent (docking score: -9.220 kcal/mol for **13a**, -7.425 kcal/mol for **13b**, -7.624 kcal/mol for **13c**, and -6.896 kcal/mol for **13d**). The favorable binding orientation of *N*-alkyl amide and pyrazolopyrimidine, coupled with fluorinated alkyl chains on the para position of the middle

phenyl ring of **11a**, resulted in a significantly enhanced inhibitory activity of **11a** (docking score: -9.451 kcal/mol for **11a**).

Fig. 1. Predicted binding modes of compound **11a** (green), **11d** (deepblue), and **13a** (blue) with TSPO (PDB:4RYI).



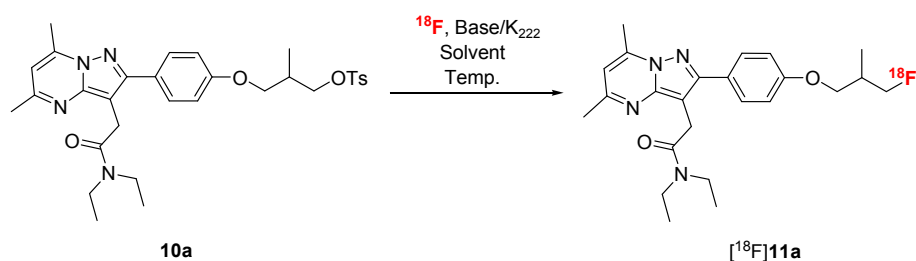
(a) Top and side views of the **11a**-TSPO docking model; (b) Detailed side view of **11a** and **11d** in the binding pocket with protein surface; (c) Detailed view of **13a** in the binding cavity. Key residues interacting with amide (yellow), pyrazolopyrimidine (sky blue), and fluoroalkyl (orange) of the compounds are highlighted. The ligands are drawn as stick-ball figures with atom coloring of nitrogen (blue), oxygen (red), and fluorine (light sky blue). The protein surface is colored blue (positive potential) and red (negative potential). Images were generated with Pymol

2.4. Radiosynthesis

Among the newly prepared ligands, [^{18}F]**11a** was chosen for an animal study because of its high binding affinity and proper lipophilicity. The radiosynthesis of [^{18}F]**11a** was performed *via* the reaction of **10a** with fluorine-18, which was produced from a cyclotron. To obtain optimal radiosynthesis conditions for [^{18}F]**11a**, several reaction factors that influenced the radiofluorination of precursor **10a** were screened. Examination of base and solvent effects on the radiofluorination showed a reaction using K_2CO_3 and K_{222} in dimethyl sulfoxide (DMSO) that produced a higher radiochemical yield (RCY) as shown in Table 2. Different quantities of base reagent were also investigated to obtain better radiofluorination results, indicating that a 1:1.5:2.8 molar ratio of precursor-base- K_{222} could produce a higher RCY. In addition, radiofluorination for 10 min afforded a higher RCY than other reaction periods.

Using the optimal radiofluorination reaction conditions, the radiosynthesis of [^{18}F]**11a** was conducted at 100 °C for 10 min, and HPLC purification was performed using ammonium acetate (NH_4OAc) and MeCN (30/70 (v/v); 0.1 M ammonium acetate/MeCN) to yield [^{18}F]**11a**, the radiolabeled target TSPO ligand, with an isolated RCY of $28.7 \pm 3.5\%$ ($n=5$, decay-corrected). In the HPLC analysis study, [^{18}F]**11a** was compared to the control ligand **11a** to validate the target radiolabeled product: the peak of the final product ([^{18}F]**11a**) was consistent with that of **11a** (Figures S1 and S2), and the HPLC peak of [^{18}F]**11a** was observed approximately 14 min after injection. In addition, the radiochemical purity of the product at the end of synthesis was greater than 99%, and specific activity was 60 GBq/ μmol ($n = 5$).

The *in vitro* stability of [^{18}F]**11a** was also investigated, and no radioactive metabolites were observed over 4 hours (Figure S3), suggesting that [^{18}F]**11a** was stable enough for *in vivo* animal study.

Table 2. Screening of reaction conditions for the radiosynthesis of precursor **10a**.^a

Entry	Base (equiv.)/K ₂₂₂ (equiv.)	Solvent	Temp. (°C)	RCY (%) ^b
1	KHCO ₃ (1.5)/K ₂₂₂ (2.8)	DMSO	100	53.4 ± 3.1
2	Cs ₂ CO ₃ (1.5)/K ₂₂₂ (2.8)	DMSO	100	37.4 ± 2.8
3	K ₂ CO ₃ (1.5)/K ₂₂₂ (2.8)	DMSO	100	70.2 ± 3.4
4	K ₂ CO ₃ (1.5)/K ₂₂₂ (2.8)	MeCN	100	41.4 ± 2.7
5	K ₂ CO ₃ (1.5)/K ₂₂₂ (2.8)	DMF	100	48.6 ± 8.5
6	K ₂ CO ₃ (1.5)/K ₂₂₂ (2.8)	DMSO	80	40.5 ± 1.7
7	K ₂ CO ₃ (1.5)/K ₂₂₂ (2.8)	DMSO	120	64.1 ± 5.2
8	K ₂ CO ₃ (1.0)/K ₂₂₂ (1.5)	DMSO	100	35.3 ± 2.5
9	K ₂ CO ₃ (1.0)/K ₂₂₂ (2.5)	DMSO	100	43.7 ± 3.7
10	K ₂ CO ₃ (1.5)/K ₂₂₂ (2.0)	DMSO	100	53.3 ± 6.4
11	K ₂ CO ₃ (1.5)/K ₂₂₂ (2.5)	DMSO	100	63.2 ± 4.5
12	K ₂ CO ₃ (1.5)/K ₂₂₂ (3.5)	DMSO	100	51.3 ± 3.2
13 ^c	K ₂ CO ₃ (1.5)/K ₂₂₂ (2.8)	DMSO	100	60.8 ± 4.8
14 ^d	K ₂ CO ₃ (1.5)/K ₂₂₂ (2.8)	DMSO	100	69.2 ± 5.3

^a Reaction conditions: precursor **10a** (3.0 mg, 5.2 μmol), solvent (250 μL), 10 min, radioactivity of [¹⁸F]fluoride: 185 MBq.

^b Radiochemical yield was determined by radio-TLC (n=3).

^c Reaction was conducted for 5 min.

^d Reaction was conducted for 20 min.

2.5. PET imaging study in an LPS-induced neuroinflammation rat model.

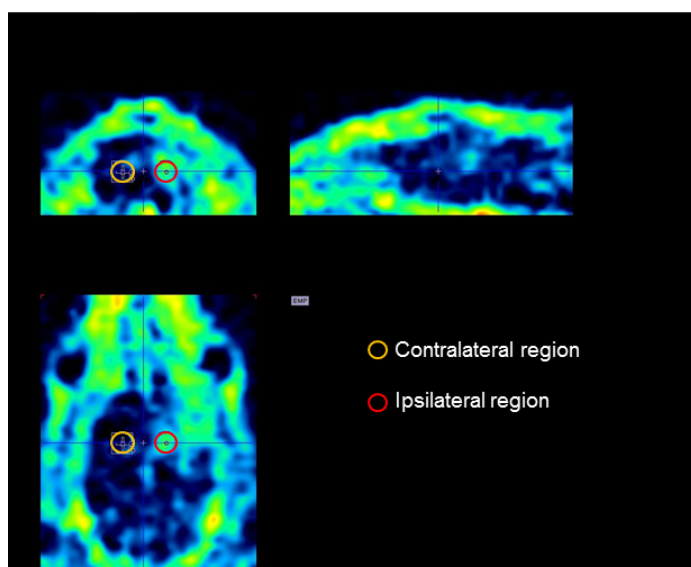
A micro-PET imaging study was performed in LPS-induced neuroinflammatory rat models to observe the potential of [¹⁸F]**11a** as a PET ligand for neuroinflammation under neuropathological conditions. Micro-PET imaging was obtained 4 days after the injection of LPS into the brain of a rat. [¹⁸F]**11a** was reconstituted in less than 5% ethanol-saline solution; the new ligand was injected through the tail vein so that it could act on the brain. A dynamic

PET scan was performed at 24 frames for 90 min to assess the behavior of [^{18}F]**11a**. Micro-PET images and time-activity curves (TACs) for the radioactivity of [^{18}F]**11a** were obtained at the contralateral and ipsilateral regions of the rat brains as shown in Fig. 2. The binding of [^{18}F]**11a** in the ipsilateral region was significantly enhanced compared to that of [^{18}F]**11a** in the contralateral region (Fig. 2a). TAC curve analysis showed that the amount of [^{18}F]**11a** was higher in the ipsilateral region compared with that of the contralateral region (Fig. 2b). [^{18}F]**11a** exhibited a 2.0-fold higher uptake ratio between the ipsilateral region and contralateral region compared with [^{18}F]DPA-714, a clinically used TSPO PET tracer (Figure S4), suggesting that the area of neuroinflammation in the brain was more clearly identified using [^{18}F]**11a** compared with [^{18}F]DPA-714 ([^{18}F]**11a** = 3.65 ± 0.28 ; [^{18}F]DPA-714 = 1.82 ± 0.19). The PET study indicated that the newly prepared TSPO ligand [^{18}F]**11a** could be a more effective PET probe to identify neuroinflammation in the brain than DPA-714.

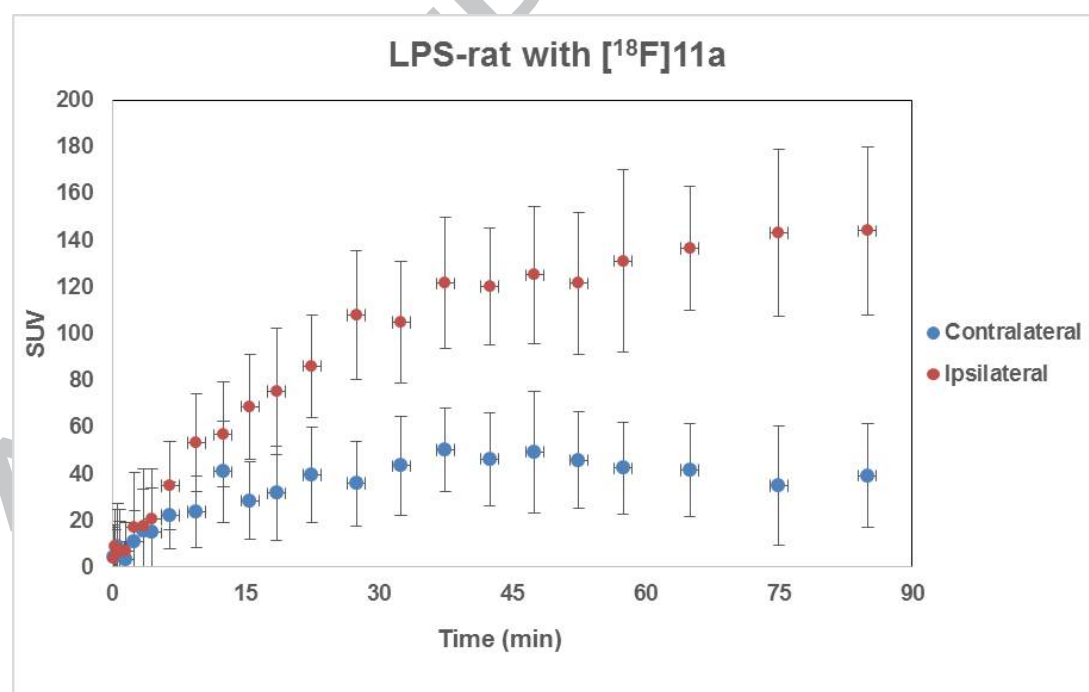
In vivo selectivity and specificity of [^{18}F]**11a** was examined *via* blockade experiments using PK11195, a previously reported TSPO PET ligand used for CNS diseases. In this experiment, PK11195 (3 mg/kg) was administered into the tail vein 60 min after the injection of [^{18}F]**11a**. The uptake of [^{18}F]**11a** was significantly reduced in the ipsilateral region of the brain by PK11195 (Fig. 3), confirming that the value of SUV decreased to a similar extent in the contralateral area after 30 min (Figure S5). These results confirmed that [^{18}F]**11a** exhibited a high specific binding capacity for TSPO in the brain.

Fig. 2. Micro-PET images and time-activity curves for the reactivity of [^{18}F]11a in a neuroinflammatory rat model injected with LPS

(a)

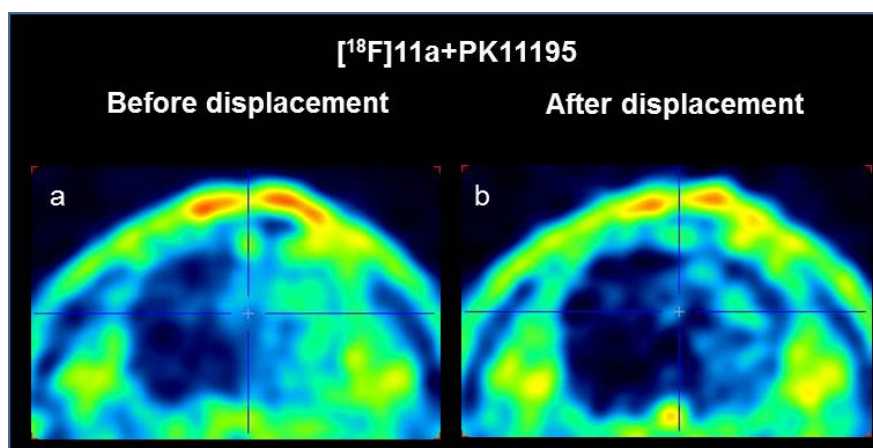


(b)



Representative micro-PET brain images and time-activity curves of radiotracers in a rat LPS model of neuroinflammation (n=3). The above image shows PET images (a) and time-activity curves (b) taken for 90 min after [^{18}F]11a injection. Ipsilateral (orange dot) and contralateral (blue dot) indicate ipsilateral and contralateral sides of the LPS-injected brain in the striatum. Data are expressed as SUV (mean and SE of three animals).

Fig. 3. Blocking study of [^{18}F]11a with PK11195.



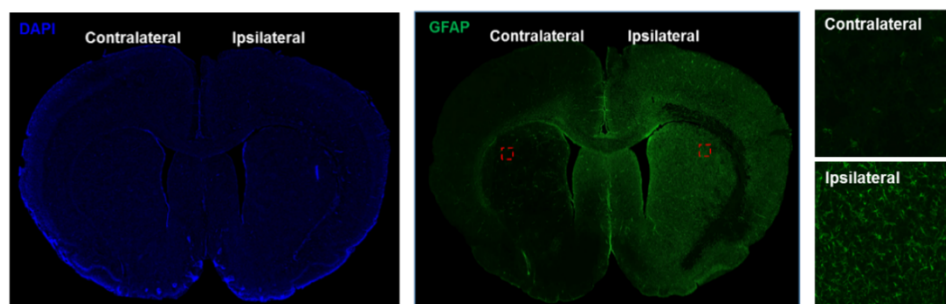
Representative coronal brain PET images (a) before and (b) after PK11195 injection.

2.6. Immunohistochemical study

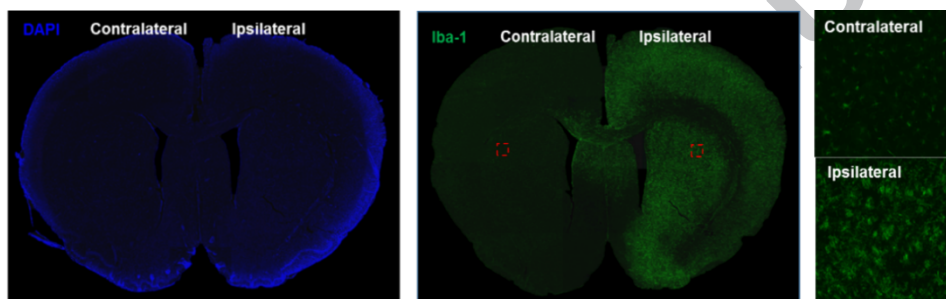
After PET scanning, LPS-injected rat brains were collected, and the neuroinflammatory response was investigated using GFAP antibody for a protein marker of reactive astrocytes, Iba-1 antibody for a protein marker of microglia, CD68 antibody for a protein marker of microglial activation, and PBR antibody for a protein marker of TSPO. The anatomical area of neuroinflammation in the brains of rats injected with LPS was successfully visualized using immunohistochemical staining (Fig. 4). Fluorescence confirmed that GFAP-positive astrocytes (Fig. 4a), Iba-1-positive microglia (Fig. 4b), CD68-positive activated microglia (Fig. 4c), and PBR-positive TSPO proteins (Fig. 4d) were increased in the ipsilateral region compared with the contralateral region of LPS-injected rat brains. The location of neuroinflammation identified using immunohistochemical staining was closely associated with [^{18}F]11a binding in the PET images. This result showed that [^{18}F]11a can potentially identify neuroinflammation in the brain using PET imaging.

Fig. 4. The immunohistochemical staining of rat brains in a neuroinflammatory rat model injected with LPS.

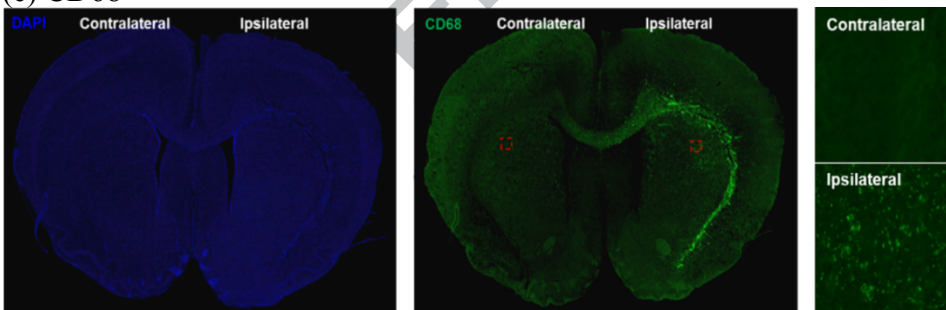
(a) GFAP



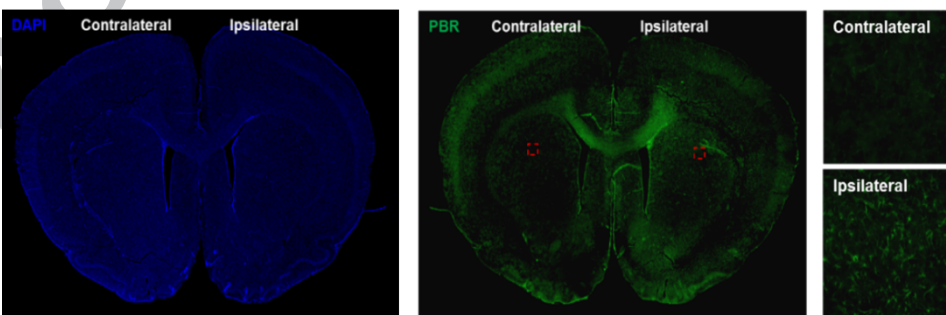
(b) Iba-1



(c) CD68



(d) PBR/TSPO



Representative images of immunohistochemistry in LPS induced neuroinflammatory animal model. Immunohistochemistry revealed that astrocytes were stained with GFAP antibody (a; green), activated microglia were stained with Iba-1 or CD68 antibody (b & c; green), or TSPO proteins were stained with PBR antibody (d; green). Nucleus was counterstained with DAPI (blue). Immunohistochemical analysis showed the significantly

increased number of GFAP-, Iba-1-, CD68- and PBR/TSPO-positive cells in the ipsilateral region compared with the contralateral region. Ipsilateral and contralateral indicate ipsilateral and contralateral region of the LPS-injected brain in the striatum.

2.7. Metabolite analysis in mouse blood and brain

The metabolites from blood and brain tissue of normal rats were analyzed at 30 min and 90 min after administration of [^{18}F]**11a** via tail vein (Figure S6). At 30 min after injection, approximately 35% of the two major polar metabolites were found in blood samples. At 90 min after injection, total metabolites increased to approximately 41%, with the majority consisting of less polar metabolites. During metabolism, polar metabolites were produced and quickly excreted from the blood vessels but did not penetrate the brain tissue. In brain tissues, approximately 96% of unchanged [^{18}F]**11a** was observed at both time points and the metabolite portions were less than 4% in brain tissue at both time points. The polar metabolites were not found in brain samples at 30 and 90 min, indicating polar metabolites did not penetrate the blood-brain barrier.

2.8. *In vitro* Cytotoxicity study

A standard WST-1 assay was used to investigate the cytotoxicity of **11a** and **13a**. SH-SY5Y cells (a human neuroblastoma cell line) were treated with various concentrations (0.1, 1, 10, 100, or 1000 nM) of **11a** or **13a** for 24 h and then the cell viability was evaluated using a WST-1 assay. The results indicated the treatment of **11a** or **13a** did not induce cytotoxic events (Figure S7).

3. Conclusions

In this study, several novel fluorinated TSPO ligands containing 2-phenylpyrazolo[1,5-*a*]pyrimidin-3-yl acetamide scaffolds were prepared. *In vitro* assays suggest that branch and

cyclic substitution could be important factors yielding high TSPO affinity; all novel ligands exhibited nano-molar TSPO affinities that were better than that of DPA-714.

Among the novel ligands, ligand **11a** was proven to be a potential ligand due to its high TSPO affinity and suitable lipophilicity. After radiosynthesis via labeling procedure with fluorine-18, [¹⁸F]**11a** was used in an animal PET imaging study to demonstrate that inflammatory lesions were visualized with a high target-to-background ratio and to confirm the high accumulation of [¹⁸F]**11a** in microglia, an enhanced TSPO expression location. Immunohistochemical study of the dissected brains validated that a high [¹⁸F]**11a** uptake region in the PET study was in agreement with the positively activated microglia location. Overall, these results illuminated [¹⁸F]**11a** as a promising TSPO PET ligand for the evaluation of neuroinflammation and other diseases related to TSPO expression.

4. Experimental section

General information was placed in Supporting Information.

4.1. Chemistry

4.1.1. General procedure for the synthesis of 2-(5,7-diethyl-2-(4-isopropoxyphenyl)pyrazolo[1,5-a]pyrimidin-3-yl)-N,N-dialkylacetamide (**4a-d**)

A mixture of the appropriate compound **3a**, **3b**, or **3c** (1.0 equiv.) and 2,4-pentanedione or 3,5-heptanedione (1.3 equiv.) in ethanol (HPLC grade, 40 mL) was stirred at reflux for 14–16 h and then evaporated. The residue was purified by flash column chromatography (ethyl acetate/hexane, 1.5:1) on silica gel to yield the desired product.

4.1.1.1. N,N-Diethyl-2-(2-(4-isopropoxyphenyl)-5,7-dimethylpyrazolo[1,5-a]pyrimidin-3-yl)acetamide (**4a**)

Treating compound **3a** (3.85 g, 11.6 mmol) with 2,4-pentanedione (1.52 g, 15.2 mmol) according to the general procedure gave compound **4a** (4.15 g, 90.6%) as a yellowish solid.

m.p. 163–165 °C; ^1H NMR (400 MHz, CDCl_3) δ 7.74 – 7.72 (m, 2H), 6.96 – 6.94 (m, 2H), 6.49 (s, 1H), 4.62 – 4.56 (m, 1H), 3.92 (s, 2H), 3.52 – 3.47 (q, $J = 6.8\text{ Hz}$, 2H), 3.43–3.38 (q, $J = 6.8\text{ Hz}$, 2H), 2.73 (s, 3H), 2.53 (s, 3H), 1.36 (d, $J = 5.6\text{ Hz}$, 6H), 1.19 (t, $J = 7.2\text{ Hz}$, 3H), 1.10 (t, $J = 6.8\text{ Hz}$, 3H); ^{13}C NMR (100 MHz, CDCl_3) δ 170.08, 158.13, 157.38, 155.20, 147.45, 144.87, 129.96, 126.03, 115.92, 108.06, 100.78, 69.88, 42.30, 40.60, 28.17, 24.54, 22.05, 16.96, 14.34, 13.08; HRMS (ESI) m/z (M+H) $^+$ calcd for $\text{C}_{23}\text{H}_{31}\text{N}_4\text{O}_2$: 395.2447; found 395.2449.

4.1.1.2. *2-(2-(4-Isopropoxyphenyl)-5,7-dimethylpyrazolo[1,5-a]pyrimidin-3-yl)-N,N-dipropylacetamide (4b)*

Treating compound **3b** (3.20 g, 8.93 mmol) with 2,4-pentanedione (1.16 g, 11.6 mmol) according to the general procedure gave compound **4b** (3.12 g, 83.6%) as a yellowish solid. m.p. 110–112 °C; ^1H NMR (400 MHz, CDCl_3) δ 7.76 – 7.72 (m, 2H), 6.96 – 6.94 (m, 2H), 6.49 (s, 1H), 4.62 – 4.58 (m, 1H), 3.92 (s, 2H), 3.37 – 3.32 (t, $J = 8.0\text{ Hz}$, 2H), 3.31 – 3.28 (t, $J = 7.6\text{ Hz}$, 2H), 2.73 (s, 3H), 2.53 (s, 3H), 1.64 – 1.62 (m, 2H), 1.55–1.52 (m, 2H), 1.38 (d, $J = 6.0\text{ Hz}$, 6H), 0.91 – 0.83 (m, 6H); ^{13}C NMR (100 MHz, CDCl_3) δ 170.57, 158.13, 157.35, 155.15, 147.51, 144.81, 129.95, 126.06, 115.93, 108.06, 100.87, 69.88, 50.00, 48.11, 28.29, 24.55, 22.28, 22.04, 16.93, 11.38, 11.26; HRMS (ESI) m/z (M+H) $^+$ calcd for $\text{C}_{25}\text{H}_{35}\text{N}_4\text{O}_2$: 423.2760; found 423.2764.

4.1.1.3. *2-(2-(4-Isopropoxyphenyl)-5,7-dimethylpyrazolo[1,5-a]pyrimidin-3-yl)-N,N-diisopropylacetamide (4c)*

Treating compound **3c** (2.70 g, 7.50 mmol) with 2,4-pentanedione (0.98 g, 9.80 mmol) according to the general procedure gave compound **4c** (2.62 g, 82.5%) as a yellowish solid. m.p. 170–172 °C; ^1H NMR (400 MHz, CDCl_3) δ 7.73 – 7.69 (m, 2H), 6.96 – 6.94 (m, 2H), 6.48 (d, $J = 0.8\text{ Hz}$, 1H), 4.61–4.58 (m, 1H), 4.24 – 4.22 (m, 1H), 3.89 (s, 2H), 3.42 – 3.40 (m, 1H), 2.72 (s, 3H), 2.54 (s, 3H), 1.37 – 1.34 (dd, $J = 6.0, 2.8\text{ Hz}$, 12H), 1.16 (d, $J = 6.4\text{ Hz}$,

6H); ^{13}C NMR (100 MHz, DMSO- d_6) δ 169.11, 158.01, 157.69, 153.85, 147.62, 144.96, 129.71, 126.02, 115.81, 108.68, 101.92, 69.57, 48.58, 45.33, 29.88, 24.61, 22.23, 20.99, 20.93, 16.76; HRMS (ESI) m/z (M+H) $^+$ calcd for $\text{C}_{25}\text{H}_{35}\text{N}_4\text{O}_2$: 423.2760; found 423.2761.

4.1.1.4. *2-(5,7-Diethyl-2-(4-isopropoxyphenyl)pyrazolo[1,5-a]pyrimidin-3-yl)-N,N-diethylacetamide (4d)*

Treating compound **3d** (4.14 g, 12.5 mmol) with 3,5-heptanedione according to the general procedure gave compound **4d** (4.37 g, 82.6%) as a yellowish solid. m.p. 84–86 °C; ^1H NMR (600 MHz, CDCl_3) δ 7.81 (d, $J = 9.0$ Hz, 2H), 6.96 (d, $J = 9.0$ Hz, 2H), 6.49 (s, 1H), 4.62 – 4.58 (m, 1H), 3.92 (s, 2H), 3.56 (q, $J = 7.2$ Hz, 2H), 3.41 (q, $J = 7.2$ Hz, 2H), 3.19 (q, $J = 7.4$ Hz, 2H), 2.82 (q, $J = 7.6$ Hz, 2H), 1.44 (t, $J = 7.2$ Hz, 3H), 1.36 – 1.32 (m, 9H), 1.21 (t, $J = 7.2$ Hz, 3H), 1.11 (t, $J = 6.9$ Hz, 3H); ^{13}C NMR (150 MHz, CDCl_3) δ 170.53, 162.29, 158.19, 155.08, 149.79, 147.74, 130.16, 126.36, 116.00, 104.91, 100.91, 69.97, 42.57, 40.80, 31.55, 28.21, 22.18, 23.43, 14.53, 13.24, 13.02, 10.45; HRMS (ESI) m/z (M+H) $^+$ calcd for $\text{C}_{25}\text{H}_{35}\text{N}_4\text{O}_2$: 423.2760; found 423.2763.

4.1.2. *General procedure for the synthesis of 2-(5,7-diethyl-2-(4-hydroxyphenyl)pyrazolo[1,5-a]pyrimidin-3-yl)-N,N-dialkylacetamide (5a–d)*

Aluminum chloride (3.3 equiv.) was added to a solution of the appropriate compound **4a**, **4b**, **4c**, or **4d** (1.0 equiv.) in anhydrous dichloromethane (50 mL). The mixture was stirred at rt for 14–16 h and treated slowly with half sat. aq. ammonium chloride (100 mL) at 0 °C. The mixture was stirred at rt for 2 h and then separated. The aqueous phase was extracted with dichloromethane (2 x 60 mL). The combined organic phase was dried over with Na_2SO_4 and evaporated. The residue was purified by flash column chromatography (dichloromethane/methanol, 20:1) on silica gel to yield the desired product.

4.1.2.1. *N,N-Diethyl-2-(2-(4-hydroxyphenyl)-5,7-dimethylpyrazolo[1,5-a]pyrimidin-3-*

yl)acetamide (5a)

Treating compound **4a** (3.93 g, 10.0 mmol) with aluminum chloride (3.99 g, 30.0 mmol) according to the general procedure gave compound **5a** (2.39 g, 67.9%) as a white solid. m.p. 247–249 °C; ¹H NMR (400 MHz, CDCl₃) δ 7.58 - 7.55 (m, 2H), 6.76 – 6.74 (m, 2H), 6.46 (d, *J* = 0.8 Hz, 1H), 3.96 (s, 2H), 3.49 – 3.47 (q, *J* = 7.2 Hz, 2H), 3.39 – 3.37 (q, *J* = 7.2 Hz, 2H), 2.71 (s, 3H), 2.54 (s, 3H), 1.15 (t, *J* = 7.2 Hz, 3H), 1.08 (t, *J* = 6.8 Hz, 3H); ¹³C NMR (100 MHz, CDCl₃) δ 170.65, 157.57, 157.36, 155.65, 147.22, 145.18, 129.82, 124.73, 115.68, 108.15, 100.21, 42.54, 40.90, 28.35, 24.34, 16.99, 14.13, 12.97; HRMS (ESI) *m/z* (M+H)⁺ calcd for C₂₀H₂₅N₄O₂: 353.1978; found 353.1975.

4.1.2.2. *2-(2-(4-Hydroxyphenyl)-5,7-dimethylpyrazolo[1,5-a]pyrimidin-3-yl)-N,N-dipropylacetamide (5b)*

Treating compound **4b** (2.11 g, 5.00 mmol) with aluminum chloride (2.00 g, 15.0 mmol) according to the general procedure gave compound **5b** (1.73 g, 90.8%) as a yellowish solid. m.p. 214–216 °C; ¹H NMR (400 MHz, CDCl₃) δ 7.60-7.57 (m, 2H), 6.78 – 6.75 (m, 2H), 6.47 (s, 1H), 3.98 (s, 2H), 3.36 – 3.27 (q, *J* = 8.0 Hz, 2H), 3.27 – 3.26 (t, *J* = 7.6 Hz, 2H), 2.72 (s, 3H), 2.54 (s, 3H), 1.59 – 1.51 (m, 4H), 0.86 – 0.81 (q, *J* = 7.6 Hz, 6H); ¹³C NMR (100 MHz, CDCl₃) δ 171.07, 157.53, 157.37, 155.69, 129.82, 124.73, 115.68, 108.12, 100.28, 50.15, 48.36, 28.56, 24.25, 22.11, 20.84, 16.99, 11.35, 11.21; HRMS (ESI) *m/z* (M+H)⁺ calcd for C₂₂H₂₉N₄O₂: 381.2291; found 381.2295.

4.1.2.3. *2-(2-(4-Hydroxyphenyl)-5,7-dimethylpyrazolo[1,5-a]pyrimidin-3-yl)-N,N-diisopropylacetamide (5c)*

Treating compound **4c** (2.03 g, 4.50 mmol) with aluminum chloride (1.98 g, 14.9 mmol) according to the general procedure gave compound **5c** (1.20 g, 70.0%) as a yellowish solid. m.p. 267 – 268 °C; ¹H NMR (400 MHz, DMSO-*d*₆) δ 7.58 – 7.56 (m, 2H), 6.84 – 6.81 (m, 3H), 4.35–4.29 (m, 1H), 3.77 (s, 2H), 3.50 – 3.48 (m, 1H), 3.33 (s, 1H) 2.68 (s, 3 H), 2.51 (s,

3H), 1.28 – 1.26 (d, $J = 6.8$ Hz, 6H), 1.16 - 1.15 (d, $J = 6.0$ Hz, 6H); ^{13}C NMR (100 MHz, DMSO- d_6) δ 169.19, 158.16, 157.55, 154.19, 147.66, 144.89, 129.70, 124.70, 115.60, 108.53, 101.05, 29.95, 24.59, 20.96, 16.76; HRMS (ESI) m/z (M+H) $^+$ calcd for $\text{C}_{22}\text{H}_{29}\text{N}_4\text{O}_2$: 381.2291; found 381.2292.

4.1.2.4. *2-(5,7-Diethyl-2-(4-hydroxyphenyl)pyrazolo[1,5-a]pyrimidin-3-yl)-N,N-diethylacetamide (5d)*

Treating compound **4d** (3.57 g, 8.45 mmol) with aluminum chloride (3.48 g, 26.2 mmol) according to the general procedure gave compound **5d** (2.87 g, 89.4%) as a yellowish solid. m.p. 207–208 °C; ^1H NMR (400 MHz, CDCl_3) δ 7.69 - 7.66 (m, 2H), 6.82 - 6.80 (m, 2H), 6.49 (s, 1H), 3.98 (s, 2H), 3.56 (q, $J = 7.2$ Hz, 2H), 3.38 (q, $J = 7.0$ Hz, 2H), 3.18 (q, $J = 7.6$ Hz, 2H), 2.83 (q, $J = 7.6$ Hz, 2H), 1.42 (t, $J = 7.5$ Hz, 3H), 1.33 (t, $J = 7.5$ Hz, 3H), 1.14 (t, $J = 6.9$ Hz, 3H), 1.07 (t, $J = 6.9$ Hz, 3H); ^{13}C NMR (150 MHz, CDCl_3) δ 171.16, 162.47, 157.56, 155.57, 150.00, 147.53, 130.03, 124.99, 115.83, 104.93, 100.30, 42.83, 41.12, 31.46, 28.57, 23.42, 14.28, 13.11, 13.06, 10.40; HRMS (ESI) m/z (M+H) $^+$ calcd for $\text{C}_{22}\text{H}_{29}\text{N}_4\text{O}_2$: 381.2291; found 381.2292.

4.1.3. *2-Methylpropane-1,3-diyl bis(4-methylbenzenesulfonate) (7)*

p-Toluenesulfonyl chloride (10.2 g, 53.2 mmol) was added to a mixture of 2-methylpropane-1,3-diol **6** (1.20 g, 13.3 mmol) and triethylamine (5.40 g, 54.3 mmol) in anhydrous dichloromethane (50 mL). The mixture was stirred at rt for 18 h. The mixture was washed with brine (80 mL) and water (80 mL), dried over with Na_2SO_4 , and evaporated. The residue was purified by flash column chromatography (ethyl acetate/hexane, 1:3) on silica gel to yield compound **7** (4.94 g, 93.1%) as a white solid. m.p. 73 – 75 °C; ^1H NMR (400 MHz, CDCl_3) δ 7.75 - 7.73 (m, 4H), 7.36 - 7.34 (d, $J = 8.4$ Hz, 4H), 3.93–3.86 (m, 4H), 2.46 (s, 6H), 2.20 – 2.12 (m, 1H), 0.92 (d, $J = 7.2$ Hz, 3H); ^{13}C NMR (150 MHz, CDCl_3) δ 145.17, 132.62,

130.07, 127.99, 70.44, 33.13, 21.78, 13.08; HRMS (ESI) m/z (M+H)⁺ calcd for C₁₈H₂₃O₆S₂: 399.0936; found 399.0939.

4.1.4. Cyclohexane-1,4-diylbis(methylene) bis(4-methylbenzenesulfonate) (**9**)

p-Toluenesulfonyl chloride (7.93 g, 41.6 mmol) was added to a mixture of 1,4-cyclohexanedimethanol (2.39 g, 16.6 mmol) and triethylamine (5.61 g, 55.4 mmol) in anhydrous dichloromethane (50 mL) at 0 °C. The mixture was stirred at rt for 15 h. The mixture was filtered and washed with H₂O (40 mL) and methanol (40 mL). The filtrate was evaporated, filtered and washed with methanol (40 mL). The combined filtered solid was washed with methanol (40 mL) and dichloromethane (2 x 15 mL) and dried to yield compound **9** (3.17 g, 42.3%) as a white solid. m.p. 160–162 °C; ¹H NMR (400 MHz, CDCl₃) δ 7.77 – 7.75 (dt, *J* = 8.4 Hz, 1.3 Hz, 4H), 7.34 – 7.32 (d, *J* = 8.0 Hz, 4H), 3.80 – 3.78 (d, *J* = 6.4 Hz, 4H), 2.44 (s, 6H), 1.74 (d, *J* = 7.2 Hz, 4H) 1.59 – 1.57 (m, 2H), 0.92 – 0.87 (m, 4H); ¹³C NMR (100 MHz, CDCl₃) δ 144.72, 133.00, 129.82, 127.86, 74.82, 36.96, 28.45, 28.03, 21.65; HRMS (ESI) m/z (M+H)⁺ calcd for C₂₂H₂₉O₆S₂: 453.1406; found 453.1408.

4.1.5. General procedure for the synthesis of 3-(4-(3-(2-(dialkylamino)-2-oxoethyl)-5,7-dimethylpyrazolo[1,5-*a*]pyrimidin-2-yl)phenoxy)-2-methylpropyl 4-methylbenzenesulfonate (**10a–c**)

The appropriate compound **5a**, **5b** or **5c** (1.0 equiv.), compound **7** (2.0 equiv.), and potassium carbonate (4.0 equiv.) were dissolved in anhydrous acetonitrile (8 mL). The mixture was stirred at 60 °C for 19–23 h. The mixture was diluted with ethyl acetate (20 mL) and washed with H₂O (20 mL). The organic phase was dried over with Na₂SO₄ and evaporated. The residue was purified by flash column chromatography (ethyl acetate/hexane, 1.5:1) on silica gel to yield the desired product.

4.1.5.1. *3-(4-(3-(2-(Diethylamino)-2-oxoethyl)-5,7-dimethylpyrazolo[1,5-a]pyrimidin-2-yl)phenoxy)-2-methylpropyl 4-methylbenzenesulfonate (10a)*

Treating compound **5a** (0.526 g, 1.50 mmol) with compound **7** (1.23 g, 3.00 mmol) according to the general procedure gave compound **10a** (0.690 g, 78.0%) as a white solid. m.p. 97–98 °C; ¹H NMR (400 MHz, CDCl₃) δ 7.76 - 7.74 (m, 4H), 7.28 - 7.27 (m, 2H), 6.86 - 6.84 (m, 2H), 6.55 (s, 1H), 4.16 - 4.12 (m, 2H), 4.01 (s, 2H), 3.90 - 3.82 (m, 2H), 3.57 - 3.51 (q, *J* = 6.8 Hz, 2H), 3.46 - 3.41 (q, *J* = 7.2 Hz, 2H), 2.79 (s, 3H), 2.62 (s, 3H), 2.42 (s, 2H), 2.36 - 2.31 (m, 1H), 1.25 (t, *J* = 7.2 Hz, 3H), 1.14 (t, *J* = 6.8 Hz, 3H), 1.10 (d, *J* = 6.8 Hz, 3H); ¹³C NMR (100 MHz, CDCl₃) δ 169.71, 158.97, 157.41, 144.81, 132.72, 129.92, 129.83, 127.84, 114.47, 107.91, 100.88, 42.33, 40.66, 33.30, 28.27, 21.64, 17.13, 14.37, 13.47, 13.10; HRMS (ESI) *m/z* (M+H)⁺ calcd for C₃₁H₃₉N₄O₅S: 579.2641; found 579.2644.

4.1.5.2. *3-(4-(3-(2-(Dipropylamino)-2-oxoethyl)-5,7-dimethylpyrazolo[1,5-a]pyrimidin-2-yl)phenoxy)-2-methylpropyl 4-methylbenzenesulfonate (10b)*

Treating compound **5b** (0.400 g, 1.05 mmol) with compound **7** (0.840 g, 2.10 mmol) according to the general procedure gave compound **10b** (0.480 g, 80.6%) as a colorless oil; ¹H NMR (400 MHz, CDCl₃) δ 7.78 - 7.74 (m, 4H), 7.29-7.28 (m, 2H), 6.85 - 6.83 (m, 2H), 6.52 (s, 1H), 4.14 - 4.12 (m, 2H), 3.95 (s, 2H), 3.90 - 3.81 (m, 2H), 3.42 (t, *J* = 8.0 Hz, 2H), 3.36 - 3.31 (m, 2H), 2.76 (s, 3H), 2.56 (s, 3H), 2.41(s, 3H), 2.37 - 2.29 (m, 1H), 1.71 - 1.62 (m, 2H), 1.62 - 1.52 (m, 2H) 1.09 (d, *J* = 7.2 Hz, 3H), 0.94 - 0.86 (m, 6H); ¹³C NMR (100 MHz, CDCl₃) δ 170.53, 158.76, 157.42, 154.93, 144.82, 132.71, 129.86, 129.84, 127.84, 126.54, 114.39, 108.13, 100.84, 49.99, 48.11, 33.30, 28.31, 24.54, 22.30, 21.64, 20.93, 16.92, 13.48, 11.40, 11.30; HRMS (ESI) *m/z* (M+H)⁺ calcd for C₃₃H₄₃N₄O₅S: 607.2954; found 607.2955.

4.1.5.3. *3-(4-(3-(2-(Diisopropylamino)-2-oxoethyl)-5,7-dimethylpyrazolo[1,5-a]pyrimidin-2-yl)phenoxy)-2-methylpropyl 4-methylbenzenesulfonate (10c)*

Treating compound **5c** (0.400 g, 1.05 mmol) with compound **7** (0.840 g, 2.10 mmol) according to the general procedure gave compound **10c** (0.298 g, 76.7%) as a colorless oil; ^1H NMR (400 MHz, CDCl_3) δ 7.77 – 7.72 (m, 4H), 7.29 – 7.28 (m, 2H), 6.85 – 6.82 (m, 2H), 6.52 (s, 1H), 4.32 – 4.25 (m, 1H), 4.14 – 4.11 (m, 2H), 3.93 (s, 2H), 3.89 – 3.81 (m, 2H), 3.48 – 3.44 (m, 1H), 2.76 (s, 3H), 2.58 (s, 3H), 2.41 (s, 3H), 2.36 – 2.29 (m, 1H), 1.39 (d, $J = 6.8$ Hz, 6H), 1.20 (d, $J = 6.8$ Hz, 6H), 1.09 (d, $J = 6.8$ Hz, 3H); ^{13}C NMR (100 MHz, CDCl_3) δ 169.47, 158.76, 157.40, 154.88, 144.82, 132.69, 129.84, 127.83, 126.51, 114.33, 108.07, 101.01, 71.51, 68.26, 48.67, 45.90, 33.29, 30.25, 24.45, 21.65, 20.91, 20.64, 16.97, 13.08; HRMS (ESI) m/z ($\text{M}+\text{H}$) $^+$ calcd for $\text{C}_{33}\text{H}_{43}\text{N}_4\text{O}_5\text{S}$: 607.2954; found 607.2958.

4.1.6. General procedure for the synthesis of 2-(5,7-diethyl-2-(4-(3-fluoro-2-methylpropoxy)phenyl)pyrazolo[1,5-*a*]pyrimidin-3-yl)-*N,N*-dialkylacetamide (**11a–c**)

The appropriate compound **11a**, **11b** or **11c** (1.0 equiv.) and tetrabutylammonium fluoride hydrate (2.0 equiv.) were dissolved in 2-methyl-2-butanol (10 mL). The mixture was stirred at 80 °C for 12–15 h. The mixture was diluted with ethyl acetate (20 mL) and washed with H_2O (20 mL). The organic phase was dried over with Na_2SO_4 and evaporated. The residue was purified by flash column chromatography (ethyl acetate/hexane, 1:5) on silica gel to yield the desired product

4.1.6.1. *N,N*-Diethyl-2-(2-(4-(3-fluoro-2-methylpropoxy)phenyl)-5,7-dimethylpyrazolo[1,5-*a*]pyrimidin-3-yl)acetamide (**11a**)

Treating compound **10a** (0.210 g, 0.350 mmol) with tetrabutylammonium fluoride hydrate (0.180 g, 0.700 mmol) according to the general procedure gave compound **11a** (0.144 g, 96.5%) as a white solid. m.p 117 – 118 °C; ^1H NMR (400 MHz, CDCl_3) δ 7.80 – 7.74 (m, 2H), 6.98–6.96 (m, 2H), 6.50 (s, 1H), 4.57 – 4.55 (m, 1H), 4.45 – 4.43 (m, 1H), 3.99 – 3.94 (m, 2H), 3.92 (s, 2H), 3.52 – 3.47 (q, $J = 7.2$ Hz, 2H), 3.43 – 3.38 (q, $J = 7.2$ Hz, 2H), 2.74 (s,

3H), 2.57(s, 3H), 2.43 – 2.30 (m, 1H), 1.22-1.20 (t, $J = 6.8$ Hz, 3H), 1.13 – 1.09 (m, 6H); ^{13}C NMR (100 MHz, CDCl_3) δ 170.03, 159.15, 157.42, 155.12, 129.97, 126.41, 114.55, 108.09, 100.80, 85.94, 84.26, 68.71, 68.66, 42.30, 40.60, 34.64, 34.45, 28.19, 24.48, 16.95, 14.34, 13.08, 12.92, 12.86; HRMS (ESI) m/z ($\text{M}+\text{H}$) $^+$ calcd for $\text{C}_{24}\text{H}_{32}\text{FN}_4\text{O}_2$: 427.2509; found 427.2505.

4.1.6.2. 2-(2-(4-(3-Fluoro-2-methylpropoxy)phenyl)-5,7-dimethylpyrazolo[1,5-a]pyrimidin-3-yl)-*N,N*-dipropylacetamide (**11b**)

Treating compound **10b** (0.200 g, 0.330 mmol) with tetrabutylammonium fluoride hydrate (0.172 g, 0.660 mmol) according to the general procedure gave compound **11b** (1.34 g, 89.4%) as a white solid. m.p 154–155 °C; ^1H NMR (400 MHz, CDCl_3) δ 7.78 – 7.74 (m, 2H), 7.98 – 6.96 (m, 2H), 6.49 (s, 1H), 4.56 – 4.45 (m, 1H), 4.45 – 4.44 (m, 1H), 3.98 – 3.96 (m, 2H), 3.92 (s, 2H), 3.38 – 3.32 (t, $J = 8.0$ Hz, 2H), 3.30 – 3.28 (m, 2H), 2.73 (s, 3H), 2.53 (s, 3H), 2.37 – 2.32 (m, 1H), 1.66 – 1.57 (m, 2H), 1.57 – 1.51 (m, 2H), 1.12 - 1.11(dd, $J = 7.2$, 1.2 Hz, 3H), 0.91 – 0.84 (m, 6H); ^{13}C NMR (100 MHz, CDCl_3) δ 170.52, 159.13, 157.40, 155.05, 147.46, 144.88, 129.96, 126.42, 114.55, 108.10, 100.89, 85.94, 84.27, 68.71, 68.65, 49.99, 48.11, 34.64, 34.45, 28.30, 24.51, 22.28, 20.93, 16.95, 12.93, 12.86, 11.39, 11.30; HRMS (ESI) m/z ($\text{M}+\text{H}$) $^+$ calcd for $\text{C}_{26}\text{H}_{36}\text{FN}_4\text{O}_2$: 455.2822; found 455.2824.

4.1.6.3. 2-(2-(4-(3-Fluoro-2-methylpropoxy)phenyl)-5,7-dimethylpyrazolo[1,5-a]pyrimidin-3-yl)-*N,N*-diisopropylacetamide (**11c**)

Treating compound **10c** (0.200 g, 0.330 mmol) with tetrabutylammonium fluoride hydrate (0.172 g, 0.660 mmol) according to the general procedure gave compound **11c** (0.138 g, 92.2%) as a white solid. m.p. 178 – 180 °C; ^1H NMR (400 MHz, CDCl_3) δ 7.75 – 7.71 (m, 2H), 6.97 – 6.95 (m, 2H), 6.49 (s, 1H), 4.57 – 4.54 (m, 1H), 4.47 – 4.44 (m, 1H), 4.28 – 4.2 (m, 1H), 4.01 – 3.92 (m, 2H), 3.91 (s, 2H), 3.43 – 3.41 (m, 1H), 2.73 (s, 3H), 2.55 (s, 3H), 2.37–2.30 (m, 1H), 1.36 (d, $J = 6.8$ Hz, 6H), 1.17 (d, $J = 6.8$ Hz, 6H), 1.10 (d, $J = 6.8$ Hz,

3H); ^{13}C NMR (100 MHz, CDCl_3) δ 169.48, 159.12, 157.37, 154.97, 129.93, 126.43, 114.48, 108.04, 101.05, 85.94, 84.27, 68.73, 68.68, 48.64, 45.89, 34.68, 34.45, 30.23, 24.48, 20.89, 20.62, 16.97, 12.92, 12.86; HRMS (ESI) m/z ($\text{M}+\text{H}$) $^+$ calcd for $\text{C}_{26}\text{H}_{36}\text{FN}_4\text{O}_2$: 455.2822; found 455.2823.

4.1.7. General procedure for the synthesis of (4-((4-(3-(2-(dialkylamino)-2-oxoethyl)-5,7-dimethylpyrazolo[1,5-a]pyrimidin-2-yl)phenoxy)methyl)cyclohexyl)methyl 4-methylbenzenesulfonate (**12a-d**)

The appropriate compound **5a**, **5b**, **5c**, or **5d** (1.0 equiv.), compound **9** (2.0 equiv.), and potassium carbonate (4.0 equiv.) were dissolved in anhydrous acetonitrile (4 mL). The mixture was stirred at 60 °C for 12–14 h. The mixture was diluted with ethyl acetate (10 mL) and washed with H_2O (10 mL). The organic phase was dried over with Na_2SO_4 and evaporated. The residue was purified by flash column chromatography (ethyl acetate/hexane, 1.5:1) on silica gel to yield the desired product.

4.1.7.1. (4-((4-(3-(2-(Diethylamino)-2-oxoethyl)-5,7-dimethylpyrazolo[1,5-a]pyrimidin-2-yl)phenoxy)methyl)cyclohexyl)methyl 4-methylbenzenesulfonate (**12a**)

Treating compound **5a** (0.410 g, 1.14 mmol) with compound **9** (1.03 g, 2.28 mmol) according to the general procedure gave compound **12a** (0.469 g, 64.9%) as a white solid. m.p. 75 °C; ^1H NMR (400 MHz, CDCl_3) δ 7.80 – 7.72 (m, 4H), 7.35 – 7.26 (m, 2H), 6.94 – 6.92 (m, 2H), 6.50 (s, 1H), 3.92 (s, 2H), 3.85 (d, J = 6.4 Hz, 2H), 3.79 (d, J = 6.0 Hz, 2H), 3.52 – 3.47 (q, J = 7.2 Hz, 2H), 3.43 – 3.37 (q, J = 7.2 Hz, 2H), 2.73 (s, 3H), 2.55 (s, 3H), 2.45 (s, 3H), 1.95–1.91 (d, J = 13.2 Hz, 2H), 1.81 – 1.78 (d, J = 12.8 Hz, 2H), 1.75–1.67 (m, 2H), 1.22 (t, J = 7.2 Hz, 3H), 1.13 (t, J = 7.2 Hz, 4H), 1.10 – 0.85 (m, 6H); ^{13}C NMR (100 MHz, CDCl_3) δ 169.98, 159.41, 157.39, 155.38, 144.64, 145.18, 133.13, 129.93, 129.81, 127.88, 126.04, 114.54, 108.02, 100.78, 75.15, 73.05, 42.30, 40.60, 37.44, 37.32, 28.79, 28.44, 28.21, 25.28,

24.32, 22.32, 21.65, 16.98, 14.34, 13.08; HRMS (ESI) m/z (M+H)⁺ calcd for C₃₅H₄₅N₄O₅S: 633.3111; found 633.3112.

4.1.7.2. (4-((4-(3-(2-(Dipropylamino)-2-oxoethyl)-5,7-dimethylpyrazolo[1,5-a]pyrimidin-2-yl)phenoxy)methyl)cyclohexyl)methyl 4-methylbenzenesulfonate (**12b**)

Treating compound **5b** (0.400 g, 1.05 mmol) with compound **9** (0.95 g, 2.10 mmol) according to the general procedure gave compound **12b** (0.500 g, 72.0%) as a white solid. m.p. 54–56 °C; ¹H NMR (400 MHz, CDCl₃) δ 7.80 – 7.72 (m, 4H), 7.36 – 7.34 (m, 2H), 6.94 – 6.91 (m, 2H), 6.50 (s, 1H), 3.94 (s, 2H), 3.86 (d, J = 8.0 Hz, 2H), 3.79 (d, J = 6.4 Hz, 2H), 3.40 – 3.36 (t, J = 7.6 Hz, 2H), 3.32 – 3.28 (t, J = 7.6 Hz, 2H), 2.74 (s, 3H), 2.55 (s, 3H), 2.45 (s, 3H), 1.91 – 1.81 (d, J = 13.2 Hz, 2H), 1.78 (d, J = 12.4 Hz, 2H), 1.77 – 1.52 (m, 6H), 1.04 – 0.98 (m, 4H), 0.91 – 0.83 (m, 6H); ¹³C NMR (100 MHz, CDCl₃) δ 170.39, 159.46, 157.37, 144.64, 133.18, 129.93, 129.81, 127.88, 125.92, 114.55, 107.96, 100.89, 75.15, 73.05, 49.98, 48.12, 37.45, 37.33, 28.80, 28.44, 28.36, 24.08, 22.25, 21.65, 20.95, 17.02, 11.40, 11.30; HRMS (ESI) m/z (M+H)⁺ calcd for C₃₇H₄₉N₄O₅S: 661.3424; found 661.3421.

4.1.7.3. (4-((4-(3-(2-(Diisopropylamino)-2-oxoethyl)-5,7-dimethylpyrazolo[1,5-a]pyrimidin-2-yl)phenoxy)methyl)cyclohexyl)methyl 4-methylbenzenesulfonate (**12c**)

Treating compound **5c** (0.400 g, 1.05 mmol) with compound **9** (0.950 g, 2.10 mmol) according to the general procedure gave compound **12c** (0.520 g, 74.9%) as a yellow solid. m.p. 158–160 °C; ¹H NMR (400 MHz, CDCl₃) δ 7.80 – 7.70 (m, 4H), 7.36 – 7.34 (m, 2H), 6.92 – 6.91 (m, 2H), 6.49 (d, J = 0.8 Hz, 1H), 4.28 – 4.21 (m, 1H), 3.89 (s, 2H), 3.85 (d, J = 8.0 Hz, 2H), 3.77 (t, J = 5.2 Hz, 2H), 3.44 – 3.40 (m, 1H), 2.73 (s, 3H), 2.55 (s, 3H), 2.45 (s, 3H), 1.94 (d, J = 13.2 Hz, 2H), 1.81 (d, J = 12.8 Hz, 2H), 1.76 – 1.52 (m, 2H), 1.36 – 1.34 (d, J = 6.8 Hz, 6H), 1.16 (d, J = 6.4 Hz, 6H), 1.10 – 0.95 (m, 4H); ¹³C NMR (100 MHz, CDCl₃) δ 169.51, 159.34, 157.37, 144.66, 133.08, 129.89, 129.82, 127.89, 126.08, 114.46, 108.04, 101.01, 75.16, 73.06, 48.64, 45.88, 37.44, 37.31, 30.24, 28.78, 28.43, 24.50, 21.67, 20.89,

20.62, 16.97; HRMS (ESI) m/z (M+H)⁺ calcd for C₃₇H₄₉N₄O₅S: 661.3424; found 661.3422.

4.1.7.4. *(4-((4-(3-(2-(Diethylamino)-2-oxoethyl)-5,7-diethylpyrazolo[1,5-a]pyrimidin-2-yl)phenoxy)methyl)cyclohexyl)methyl 4-methylbenzenesulfonate (12d)*

Treating compound **5d** (0.100 g, 0.263 mmol) with compound **9** (0.234 g, 517 μmol) according to the general procedure gave compound **12d** (0.131 g, 75.1%) as a white solid. m.p. 104 – 107 °C; ¹H NMR (400 MHz, CDCl₃) δ 7.76 – 7.75 (m, 4H), 7.36 – 7.34 (m, 2H), 6.95 – 6.92 (m, 2H), 6.50 (s, 1H), 3.91 (s, 2H), 3.85 (d, $J = 6.4$ Hz, 2H), 3.78 (d, $J = 6.4$ Hz, 2H), 3.58 – 3.52 (q, $J = 7.2$ Hz, 2H), 3.44 – 3.37 (q, $J = 7.2$ Hz, 2H), 3.21 – 3.15 (q, $J = 7.6$ Hz, 2H), 2.84 – 2.78 (q, $J = 7.6$ Hz, 2H), 2.45 (s, 3H), 1.95 (d, $J = 13.2$ Hz, 2H), 1.81 (d, $J = 12.0$, 2H), 1.75 – 1.64 (m, 2H), 1.43 (t, $J = 7.6$ Hz, 3H), 1.32 (t, $J = 7.6$ Hz, 3H), 1.20 (t, $J = 6.8$ Hz, 3H), 1.00 (t, $J = 6.8$ Hz, 3H), 1.04 – 0.87 (m, 4H); ¹³C NMR (100 MHz, CDCl₃) δ 170.37, 162.20, 159.27, 154.88, 149.72, 144.74, 144.67, 133.05, 132.96, 129.98, 129.82, 127.91, 126.38, 114.48, 104.82, 100.74, 75.19, 74.82, 73.01, 42.44, 40.66, 37.42, 37.31, 36.95, 31.40, 28.79, 28.44, 28.02, 23.32, 21.68, 14.42, 13.13, 12.92, 10.32; HRMS (ESI) m/z (M+H)⁺ calcd for C₃₇H₄₉N₄O₅S : 661.3424; found 661.3425.

4.1.8. *General procedure for the synthesis of N,N-dialkyl-2-(2-(4-((4-(fluoromethyl)cyclohexyl)methoxy)phenyl)-5,7-dimethylpyrazolo[1,5-a]pyrimidin-3-yl)acetamide (13a–d)*

The appropriate compound **12a**, **12b**, **12c**, or **12d** (1.0 equiv.) and tetrabutylammonium fluoride hydrate (2.0 equiv.) were dissolved in 2-methyl-2-butanol (10 mL). The mixture was stirred at 80 °C for 14–15 h. The mixture was diluted with ethyl acetate (20 mL) and washed with H₂O (20 mL). The organic phase was dried over with Na₂SO₄ and evaporated. The residue was purified by flash column chromatography (ethyl acetate/hexane, 1:1) on silica gel to yield the desired product.

4.1.8.1. *N,N*-diethyl-2-(2-(4-((4-(fluoromethyl)cyclohexyl)methoxy)phenyl)-5,7-dimethylpyrazolo[1,5-*a*]pyrimidin-3-yl)acetamide (**13a**)

Treating compound **12a** (0.150 g, 0.240 mmol) with tetrabutylammonium fluoride hydrate (0.180 g, 0.700 mmol) according to the general procedure gave compound **13a** (0.0940 g, 81.4%) as a white solid. m.p. 139 – 140 °C; ¹H NMR (400 MHz, CDCl₃) 7.76 – 7.73 (m, 4H), 6.97 – 6.95 (m, 2H), 6.50 (s, 1H), 4.33 (d, *J* = 6.0 Hz, 2H), 4.21 (d, *J* = 6.0 Hz, 2H), 3.93 (s, 2H), 3.83 (d, *J* = 6.4 Hz, 2H), 3.53 – 3.47 (q, *J* = 7.2 Hz, 2H), 3.43 – 3.38 (q, *J* = 7.2 Hz, 2H), 2.74 (s, 3H), 2.55 (s, 3H), 1.99-1.97 (d, *J* = 9.2 Hz, 2H), 1.87-1.85 (d, *J* = 10.0 Hz, 2H), 1.83 – 1.71 (m, 2H), 1.22-1.18 (m, 4H), 1.16 – 1.07 (m, 6H); ¹³C NMR (100 MHz, CDCl₃) δ 169.98, 159.41, 157.39, 155.38, 144.64, 145.18, 133.13, 129.93, 129.81, 127.88, 126.04, 114.54, 108.02, 100.78, 75.15, 73.05, 42.30, 40.60, 37.44, 37.32, 28.79, 28.44, 28.21, 25.28, 24.32, 22.32, 21.65, 16.98, 14.34, 13.08; HRMS (ESI) *m/z* (M+H)⁺ calcd for C₂₈H₃₈FN₄O₂ : 481.2979; found 481.2981.

4.1.8.2. 2-(2-(4-((4-(Fluoromethyl)cyclohexyl)methoxy)phenyl)-5,7-dimethylpyrazolo[1,5-*a*]pyrimidin-3-yl)-*N,N*-dipropylacetamide (**13b**)

Treating compound **12b** (0.150 g, 0.230 mmol) with tetrabutylammonium fluoride hydrate (0.120 g, 0.460 mmol) according to the general procedure gave compound **13b** (0.102 g, 87.1%) as a yellow oil; ¹H NMR (400 MHz, CDCl₃) δ 7.76 – 7.73 (m, 2H), 6.97 – 6.95 (m, 2H), 6.50 (s, 1H), 4.32 (d, *J* = 5.6 Hz, 1H), 4.21 (d, *J* = 6.0 Hz, 1H), 3.93 (s, 2H), 3.81 (d, *J* = 6.4 Hz, 2H), 3.40 – 3.36 (t, *J* = 7.6 Hz, 2H), 3.33 – 3.28 (t, *J* = 7.2 Hz, 2H), 2.74 (s, 3H), 2.54 (s, 3H), 2.00 – 1.98 (d, *J* = 8.8 Hz, 2H), 1.87 - 1.85 (d, *J* = 10.0 Hz, 2H), 1.82 – 1.71 (m, 2H), 1.70–1.63 (m, 2H), 1.59 – 1.52 (m, 2H), 1.14 – 1.07 (m, 4H), 0.91 – 0.84 (m, 6H); ¹³C NMR (100 MHz, CDCl₃) δ 170.54, 159.45, 157.38, 155.16, 129.91, 126.08 114.56, 108.06, 100.85, 89.33, 87.66, 73.24, 49.99, 48.11, 38.73, 38.56, 37.63, 28.96, 28.32, 27.87, 27.81, 24.48, 22.27, 20.92, 16.95, 11.40, 11.29; HRMS (ESI) *m/z* (M+H)⁺ calcd for C₃₀H₄₂FN₄O₂ :

509.3292; found 509.3289.

4.1.8.3. 2-(2-(4-((4-(Fluoromethyl)cyclohexyl)methoxy)phenyl)-5,7-dimethylpyrazolo[1,5-*a*]pyrimidin-3-yl)-*N,N*-diisopropylacetamide (**13c**)

Treating compound **12c** (0.150 g, 0.240 mmol) with tetrabutylammonium fluoride hydrate (0.120 g, 0.460 mmol) according to the general procedure gave compound **13c** (0.204 g, 90.2%) as a white solid. m.p. 160–162 °C; ¹H NMR (400 MHz, CDCl₃) δ 7.73–7.71 (m, 2H), 6.96–6.94 (m, 2H), 6.50 (s, 1H), 4.32 – 4.31 (d, *J* = 6.0 Hz, 1H), 4.30 – 4.23 (m, 1H), 4.20 – 4.19 (d, *J* = 6.0 Hz, 1H), 3.90 (s, 2H), 3.80 (d, *J* = 6.4 Hz, 2H), 3.43 (m, 1H), 2.73 (s, 3H), 2.55 (s, 3H), 2.01–1.99 (d, *J* = 9.2 Hz, 2H), 1.89 – 1.84 (d, *J* = 9.6 Hz, 2H), 1.82 – 1.70 (m, 2H), 1.37 – 1.35 (d, *J* = 6.8 Hz, 6H), 1.17 (d, *J* = 6.4 Hz, 6H), 1.17 – 1.03 (m, 4H); ¹³C NMR (100 MHz, CDCl₃) δ 169.50, 159.42, 157.37, 155.07, 144.66, 129.89, 126.08, 114.49, 108.07, 101.01, 89.35, 89.14, 87.69, 73.24, 48.65, 45.90, 38.73, 38.54, 37.62, 30.24, 28.94, 27.86, 27.80, 24.46, 21.07, 20.89, 20.63, 16.97; HRMS (ESI) *m/z* (M+H)⁺ calcd for C₃₀H₄₂FN₄O₂: 509.3292; found 509.3291.

4.1.8.4. 2-(5,7-Diethyl-2-(4-((4-(fluoromethyl)cyclohexyl)methoxy)phenyl)pyrazolo[1,5-*a*]pyrimidin-3-yl)-*N,N*-diethylacetamide (**13d**)

Treating compound **12d** (0.260 g, 0.393 mmol) with tetrabutylammonium fluoride hydrate (0.210 g, 0.803 mmol) according to the general procedure gave compound **13d** (0.176 g, 87.9%) as a white solid. m.p. 108–110 °C; ¹H NMR (400 MHz, CDCl₃) δ 7.82–7.79 (dd, *J* = 8.8, 2.4 Hz, 2H), 6.98–6.95 (d, *J* = 8.8 Hz, 2H), 6.50 (s, 1H), 4.33 (d, *J* = 6.4 Hz, 1H), 4.21 (d, *J* = 6.0 Hz, 1H), 3.92 (s, 2H), 3.81 (d, *J* = 6.4 Hz, 2H), 3.56 (q, *J* = 7.2 Hz, 2H), 3.41 (q, *J* = 6.8 Hz, 2H), 3.20 (q, *J* = 7.6 Hz, 2H), 2.83 (q, *J* = 7.6 Hz, 2H), 2.00 – 1.98 (d, *J* = 9.2 Hz, 2H), 1.87–1.84 (d, *J* = 9.6 Hz, 2H), 1.81 – 1.70 (m, 2H), 1.44 (t, *J* = 7.6 Hz, 3H), 1.33 (t, *J* = 7.2 Hz, 3H), 1.21 (t, *J* = 7.2 Hz, 3H), 1.14 – 1.06 (m, 7H); ¹³C NMR (100 MHz, CDCl₃) δ 170.37, 162.19, 159.35, 154.91, 149.70, 147.56, 129.98, 126.27, 114.81, 104.81, 100.74,

89.38, 87.71, 73.20, 42.44, 40.66, 38.73, 38.55, 37.60, 31.41, 28.95, 28.13, 27.81 (d, $J = 5.7$ Hz), 23.32, 14.42, 13.13, 12.92, 10.33; HRMS (ESI) m/z (M+H)⁺ calcd for C₃₀H₄₂FN₄O₂: 509.3292; found 509.3295.

4.2. *In vitro* binding assay

The affinity of 2-phenylpyrazolo[1,5-*a*]pyrimidin-3-ylacetamide derivatives (**11a–c** and **13a–d**) and DPA-714 as a reference ligand for TSPO were evaluated with little modification to the previously published procedure.^[32] Leukocytes were obtained and cryopreserved from 200 mL of heparinized whole blood via Ficoll-Hypaque density centrifugation using a Lymphocyte Separation Medium (Lonza, Walkersville, MD, U.S.A.) according to the manufacturer's guidance. Before the day of the assay, the cells were thawed, diluted with an equal volume of buffer (50 mM HEPES, pH 7.4), homogenized with a Teflon pestle, and centrifuged at 20,000 $\times g$ for 15 min at 4 °C. The resulting crude membrane pellet was resuspended in 2.4 mL buffer and stored at –70 °C. The Bradford Protein Assay (Bio-Rad, Hercules, CA, U.S.A.) was used to determine the protein concentration. For the saturation binding assay, leukocytes (100 μ L resuspended membranes) were added to a mixture of 100 μ L of 3 μ M TSPO radioligand (³H]PK11195, specific radioactivity: 3.08 GBq/ μ mol; IC₅₀ = 1.40 \pm 0.4 nM) and 10% ethanol in a final volume of 1 mL. For the inhibition experiments, 1 mL of the reaction mixture containing 50 μ L of each derivative (0.124–10,000 nM in 10% ethanol) and 0.70 nM [³H]PK11195 in 10% ethanol was incubated for 30 min at r.t. for the binding assay. The reaction mixture was filtered using Whatman GF/A glass filters and washed with 10% ethanol (2 \times 3 mL). Radioactivity retained on the filter was measured using a β -counter. Under the assay conditions, the percentage of the specific binding portion was less than 20% of the total ³H radioactivity. Results of the inhibition and saturation studies

were employed for nonlinear regression analysis using PRISM software to estimate the K_i values of the novel small molecules (**11a–c** and **13a–d**) and DPA-714.

4.3. Lipophilicity

The lipophilicity ($\log P_{7.5}$ values) of compounds **11a–c**, **13a–d** was examined using a previously described HPLC method.^[38] Phosphate buffer (0.1 M) was prepared by dissolving weighed quantities of potassium dihydrogen orthophosphate in HPLC-grade water and adjusting the pH to 7.5 with sodium hydroxide solution (0.1 M). Samples were analyzed with a ZORBAX Eclipse XDB-C18 column (Agilent, 150 x 4.6 mm) using a mobile phase of MeOH and phosphate buffer (85/15 (v/v), pH = 7.5) with a flow rate of 1.0 mL/min. The lipophilicity of each ligand was calculated by comparing its retention time (t_R) with standards having known $\log P_{7.5}$ values. The standards were aniline, benzene, bromobenzene, ethyl benzene, trimethylbenzene, and hexachlorobenzene dissolved in the mobile phase. All sample injections were performed in triplicate and the results were averaged to obtain the final values. A calibration curve of $\log P_{7.5}$ versus \log relative t_R (to aniline) was generated and the equations were polynomial with an R^2 of 0.996 or greater.

4.4. Radiosynthesis

No-carrier added [^{18}F]fluoride was produced by the $^{18}\text{O}(\text{p},\text{n})^{18}\text{F}$ reaction using H_2^{18}O as a target material in the cyclotron (11 MeV). The bombarded target liquid was passed through QMA light (Waters, USA) to isolate [^{18}F]fluoride anions. [^{18}F]Fluoride was released into the reaction vessel by the elution of catalyst solution (Cryptand 222 5.46 mg and K_2CO_3 1.07 mg in H_2O 0.1 mL and acetonitrile 0.3 mL). The solution was dried by azeotropic distillation under argon stream and repeated with the extra addition of acetonitrile (0.2 mL x 3).

Precursor (**10a**) solution (3 mg, 5.19 μmol in DMSO 0.25 mL) was added to the reaction vessel and heated at 100 °C. Afterwards, the reaction solution was diluted with 0.5 mL acetonitrile for the prep-HPLC injection. [^{18}F]**11a** was finely separated by a semi-preparative HPLC column (YMC-Pack ODS-A, C18 silica gel, 10 \times 250 mm, 5 μm) and eluents (100 mM NH_4OAc buffer and acetonitrile, 30:70 ratio). The product fraction was collected between 14.0~14.5 min using a UV detector at 254 nm and a gamma-ray detector.

4.5. PET imaging study in LPS-induced neuroinflammation

4.5.1. Micro-PET imaging protocol and Blocking study

The animals used in this experiment were handled using the Guidelines for Animal Experimentation. This study was approved by the Ethics Committee of Gachon University Animal Care and Use (GIACUC-R2018011). Male Sprague-Dawley (SD) rats (230 g, Daehanbiolink Co. Ltd, Chungbuk, Republic of Korea) were induced to neuro-inflammation with lipopolysaccharide (LPS; Sigma-Aldrich, St. Louis, MO, USA). Four days after LPS injection, three rats were studied for brain micro-PET imaging. All rats were fasted 2 h prior to the experiment to improve [^{18}F]**11a** uptake in the brain. The rats were anesthetized with 5% isoflurane prior to scanning and were maintained in 2.5% isoflurane at 80% O_2 after the injection of [^{18}F]**11a** and placed in the micro-PET to minimize stress; injections were administered within 5 min. Micro-PET images were obtained using a dedicated animal PET (Concorde Microsystems, Knoxville, Tennessee, USA). Micro-PET acquisition in the list mode was initiated immediately following the intravenous injection of [^{18}F]**11a**. At the end of each study, the list mode data was sorted into a dynamic scan consisting of 24 frames such as 15s*4, 60s*4, 180s*5, 300s*8, 600s*3. The acquired images were reconstructed using the 3D Adjoint Monte Carlo method combined with scattering and random corrections.

For the blocking experiments, PK11195 (3 mg/kg) dissolved in 1020 μL of saline containing

10% ethanol (120 μ L) and 5% Tween 80 (60 μ L) was administrated 60 min after the PET scans with [18 F]**11a** were started. This protocol was approved by the Ethics Committee of Gachon University Neuroscience Research Institutional Animal Care and Use (NRI-IACUC-2018-002).

4.5.2. Micro-PET image data analysis

Analysis of the PET images was performed using PMOD software v.3.6 (PMOD Technologies Ltd., Zurich, Switzerland). A strongly visualized area in the summed image of all frames set a volume of interest (VOI) of 1.2 mm radius on the striatum of the ipsilateral region and the symmetrical area defined as the contralateral region. The amount of radioactive tracer uptake in each ROI was analyzed as a percentage of the dose per cubic centimeter (% ID/cc) and the time-activity curve (TAC), indicating that the change in radioligand concentration over time was evaluated for the ipsilateral/contralateral region.

4.6. Immunohistochemical study

After completing PET imaging, rats were anesthetized with Zoletil 50 (50 mg/kg) and Rumpun (0.2 mg/kg) and were transcardially perfused by saline with heparin. Mice brains were collected and fixed in 4% paraformaldehyde for 24 h and were dehydrated in 30% sucrose. After freezing using an OCT compound, the striatum region was sectioned to a thickness of 30 μ m at -20 $^{\circ}$ C using a cryotome (LEICA biosystmes, Nussloch, Germany). After three washes with PBS-T (0.4% Triton X-100 and PBS) for 10 min, blocking was performed with PBS-T added 10% NGS, 3% BSA for 30 min at room temperature. Primary antibodies (GFAP (DAKO, USA), Iba-1 (NOVUS, USA), CD68 (Abcam, UK) or PBR (NOVUS, USA) antibody) were incubated overnight at 4 $^{\circ}$ C. After washing three times, appropriate secondary antibodies were incubated at room temperature for 1 h. After washing three times, mounting was performed using fluorescence mounting medium (Dako, Denmark)

with DAPI (Vector, USA). Tissue images were observed using an ECLIPSE TS2 fluorescence microscope (Nikon, Japan) and pictures were obtained using NIS-Element BR 4.40.

4.7. Radiolabeled metabolite analysis in mice

Normal Sprague-Dawley (SD) rats were injected intravenously *via* the tail vein with [¹⁸F] **11a** (approximately 3 mCi/200 μ L, 10% EtOH/saline) and then sacrificed at 30 min and 90 min (n = 3 for each time point) after injection. Blood samples were immediately obtained and placed into an ice-cooled container. The blood samples were centrifuged at 15,000g for 2 min at 4°C. The supernatant (0.2 mL) was collected in a tube containing acetonitrile (0.2 mL), and the resulting mixture was vortexed for 15 sec and then centrifuged at 15,000g for 2 min. The brain samples were homogenized under ice-cold conditions. The brain samples were centrifuged at 15,000g for 2 min at 4°C. The supernatant (0.5 mL) was collected in a tube containing acetonitrile (0.5 mL) and centrifuged at 15,000g for 2 min. Samples were repeatedly spotted (10–15 times) on TLC plates using a micropipette (1 μ L) based on the radioactivity. TLC plates were developed using an eluent mixture (CH₂Cl₂:MeOH = 10:1). TLC analysis was performed using the Bioscam AR-2000 radio-TLC scanner, and radiochemical identity and purity were determined.

4.8. Cell culture and cell viability assay

SH-SY5Y cells were cultured in DMEM (Wellgene, Republic of Korea) containing 10% FBS (GE Healthcare Hyclone, USA) and 1% penicillin/streptomycin mixture (Gibco, USA). SH-SY5Y cells were cultured in a 5% CO₂ humidified incubator at 37°C. SH-SY5Y cells (3 \times 10³ cells/wells) were plated on 96-well plates and experiments were performed one day later. To measure the cell viability, WST-1 (Roche, Switzerland) assay was performed according to the

manufacturer's instructions. Various concentrations (0.1, 1, 10, 100, or 1000 nM) of **11a** or **13a** were added to the media and cultured for 24 h (DMSO was used as a negative control). Then, WST-1 reagent was added to each well and SH-SY5Y cells were incubated at 37°C in 5% CO₂ for 2 h. The absorbance of the samples treated with the control, **11a**, and **13a** was measured at optical density (OD) of 450 nm using a multilabel plate reader (PerkinElmer, VICTOR X4, German). All values are expressed as the mean ± standard error of the mean (SEM). All statistical analyses were performed using GraphPad Prism 8 (GraphPad Software, CA, USA). The statistical analyses were performed using one-way ANOVA, and P-values < 0.05 were considered statistically significant.

Acknowledgments

This research was supported by Basic Science Research Program through the National Research Foundation of Korea (NRF) funded by the Ministry of Education (2018R1D1A1B07047572). This work was supported by Fund of Biomedical Research Institute, Chonbuk National University Hospital. This work was supported by a grant from the Korea Health Technology R & D Project through the Korea Health Industry Development Institute (KHIDI), funded by the Ministry for Health and Welfare, Korea (HI14C1135).

Conflict of interest

The authors declare no conflict of interest.

Appendix A. Supplementary data

Supplementary data related to this article can be found at.

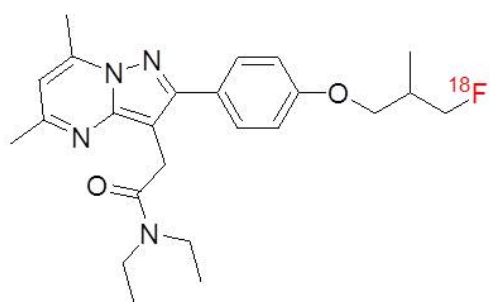
References

- [1] Miller PW, Long NJ, Vilar R, Gee AD. Synthesis of ^{11}C , ^{18}F , ^{15}O , and ^{13}N radiolabels for positron emission tomography. *Angew Chem Int Ed*. 2008;47:8998–9033.
- [2] Tredwell M, Gouverneur V. ^{18}F labeling of arenes. *Angew Chem Int Ed*. 2012;51:11426–11437.
- [3] Ametamey SM, Honer M, Schubiger PA. Molecular imaging with PET. *Chem Rev*. 2008;108:1501–1516.
- [4] Jacobson O, Kiesewetter DO, Chen X. Fluorine-18 radiochemistry, labeling strategies and synthetic routes. *Bioconjugate Chem*. 2015;26:1–18.
- [5] Gillis EP, Eastman KJ, Hill MD, Donnelly DJ, Meanwell NA. Applications of fluorine in medicinal chemistry. *J Med Chem*. 2015;58:8315–8359.
- [6] Papadopoulos V, Baraldi M, Guilarte TR, et al. *Trends Pharmacol Sci*. 2006;27:402–409.
- [7] Ory D, Postnov A, Koole M, et al. Quantification of TSPO overexpression in a rat model of local neuroinflammation induced by intracerebral injection of LPS by the use of [^{18}F]DPA-714 PET. *Eur J Nucl Med Mol Imaging*. 2016;43:163–172.
- [8] Cosenza-Nashat M, Zhao M-L, Suh H-S, et al. Expression of the translocator protein of 18 kDa by microglia, macrophages and astrocytes based on immunohistochemical localization in abnormal human brain. *Neuropathol Appl Neurobiol*. 2009;35:306–328.
- [9] Venetti S, Lopresti BJ, Wiley CA. The peripheral benzodiazepine receptor (translocator protein 18 kDa) in microglia: From pathology to imaging. *Prog Neurobiol*. 2006;80:308–322.
- [10] Lavisse S, Guillemier M, Hérard A-S, et al. Reactive astrocytes overexpress TSPO and are detected by TSPO positron emission tomography imaging. *J Neurosci*. 2012;32:10809–10818.
- [11] Yasuno F, Ota M, Kosaka J, et al. Increased binding of peripheral benzodiazepine receptor in alzheimer's disease measured by positron emission tomography with [^{11}C]DAA1106. *Biol Psychiatry*. 2008;64:835–841.

- [12] Le Fur G, Perrier ML, Vaucher N, et al. Peripheral benzodiazepine binding sites: effect of PK 11195, I-(2-chlorophenyl)-N-methyl-N-(1-methylpropyl)-3-isoquinolinecarboxamide. *Life Sci.* 1983;32:1839–1847.
- [13] Camsonne R, Crouzel C, Comar D, et al. Synthesis of N-(¹¹C) methyl, N-(methyl-1 propyl), (chloro-2 phenyl)-1 isoquinoline carboxamide-3 (PK 11195) : A new ligand for peripheral benzodiazepine receptors. *J Labelled Compd Radiopharm.* 1984;21:985–991.
- [14] Chauveau F, Boutin H, Van Camp N, Dollé F, Tavitian B. Nuclear imaging of neuroinflammation: a comprehensive review of [¹¹C]PK11195 challengers. *Eur J Nucl Med Mol Imaging.* 2008;35:2304–2319
- [15] Kreisl WC, Fujita M, Fujimura Y, et al. Comparison of [¹¹C]-(R)-PK 11195 and [¹¹C]PBR28, two radioligands for translocator protein (18 kDa) in human and monkey: Implications for positron emission tomographic imaging of this inflammation biomarker. *NeuroImage.* 2010;49:2924–2932.
- [16] Damont A, Roeda D, Dollé F. The potential of carbon-11 and fluorine-18 chemistry: Illustration through the development of positron emission tomography radioligands targeting the translocator protein 18 kDa. *J Label Compd Radiopharm.* 2013;56:96–104.
- [17] Zhang M-R, Maeda J, Furutsuka K, et al. [¹⁸F]FMDAA1106 and [¹⁸F]FEDAA1106: Two positron-emitter labeled ligands for peripheral benzodiazepine receptor (PBR). *Bioorg Med Chem Lett.* 2003;13:201–204
- [18] James ML, Fulton RR, Vercoullie J. DPA-714, a New translocator protein-specific ligand: synthesis, radiofluorination, and pharmacologic Characterization. *J Nucl Med.* 2008; 49:814–822.
- [19] Blair A, Zmuda F, Malviya, G, et al. A novel ¹⁸F-labelled high affinity agent for PET imaging of the translocator protein. *Chem Sci.* 2015;6:4772–4777.

- [20] Wadsworth H, Jones PA, Chau W-F, et al. [¹⁸F]GE-180: A novel fluorine-18 labelled PET tracer for imaging Translocator protein 18 kDa (TSPO). *Bioorg Med Chem Lett*. 2012;22:1308–1313.
- [21] Wilson AA, Garcia A, Parkes J, et al. Radiosynthesis and initial evaluation of [¹⁸F]-FEPPA for PET imaging of peripheral benzodiazepine receptors. *Nucl Med Biol*. 2008;35:305–314.
- [22] Leaver KR, Reynolds A, Bodard S, et al. Effects of translocator protein (18 kDa) ligands on microglial activation and neuronal death in the quinolinic-acid-injected rat striatum. *ACS Chem Neurosci*. 2012;3:114–119.
- [23] Arlicot N, Vercouillie J, Ribeiro M-J, et al. Initial evaluation in healthy humans of [¹⁸F]DPA-714, a potential PET biomarker for neuroinflammation. *Nucl Med Biol*. 2012;39:570–578.
- [24] Peyronneau M-A, Saba W, Goutal S, et al. Metabolism and quantification of [¹⁸F]DPA-714, a new TSPO positron emission tomography radioligand. *Drug Metab Dispos*. 2013;41:122–131.
- [25] Lavisse S, Inoue K, Jan C, et al. [¹⁸F]DPA-714 PET imaging of translocator protein TSPO (18 kDa) in the normal and excitotoxically-lesioned nonhuman primate brain. *Eur J Nucl Med Mol Imaging*. 2015;42:478–494.
- [26] Selleri S, Bruni F, Costagli C, et al. 2-Arylpyrazolo[1,5-*a*]pyrimidin-3-yl acetamides. New potent and selective peripheral benzodiazepine receptor ligands. *Bioorg Med Chem*. 2001;9:2661–2671.
- [27] Selleri S, Gratteri P, Costagli C, et al. Insight into 2-phenylpyrazolo[1,5-*a*]pyrimidin-3-yl acetamides as peripheral benzodiazepine receptor ligands: Synthesis, biological evaluation and 3D-QSAR investigation. *Bioorg Med Chem*. 2005;13:4821–4834.

- [28] Banister SD, Wilkinson SM, Hanani R, et al. A practical, multigram synthesis of the 2-(2-(4-alkoxyphenyl)-5,7-dimethylpyrazolo[1,5-*a*]pyrimidin-3-yl)acetamide (DPA) class of high affinity translocator protein (TSPO) ligands. *Tetrahedron Lett.* 2012;53:3780–3783.
- [29] Médran-Navarrete V, Damont A, Peyronneau M-A, et al. Preparation and evaluation of novel pyrazolo[1,5-*a*]pyrimidine acetamides, closely related to DPA-714, as potent ligands for imaging the TSPO 18 kDa with PET. *Bioorg Med Chem Lett.* 2014;24:1550–1556.
- [30] Banister SD, Beinat C, Wilkinson SM, et al. Ether analogues of DPA-714 with subnanomolar affinity for the translocator protein (TSPO). *Eur J Med Chem.* 2015;93:392–400.
- [31] Damont A, Médran-Navarrete V, Cacheux F, et al. Novel pyrazolo[1,5-*a*]pyrimidines as translocator protein 18 kDa (TSPO) ligands: Synthesis, *in vitro* biological evaluation, [¹⁸F]-labeling, and *in vivo* neuroinflammation PET images. *J Med Chem.* 2015;58:7449–7464.
- [32] Kwon Y-D, Kang S, Park H, et al. Novel potential pyrazolopyrimidine based translocator protein ligands for the evaluation of neuroinflammation with PET. *Eur J Med Chem.* 2018;159:292–306.
- [33] Guo Y, Kalathur RC, Liu Q, et al. Hendrickson, Structure and activity of tryptophan-rich TSPO proteins, *Science* 2015;347:551-555.
- [34] Jaremko L, Jaremko M, Giller K, et al. Structure of the mitochondrial translocator protein in complex with a diagnostic ligand, *Science* 2014;343:1363-1366.

**[¹⁸F]11a**